Distributed Space-Time-Frequency Block Code for Cognitive Wireless Relay Networks

Quoc-Tuan Vien, Brian G. Stewart, Huan X. Nguyen and Orhan Gemikonakli

Abstract

In this paper, we consider cooperative transmission in cognitive wireless relay networks (CWRNs) over frequency-selective fading channels. We propose a new distributed space-time-frequency block code (DSTFBC) for a two-hop nonregenerative CWRN, where a primary source node and multiple secondary source nodes convey information data to their desired primary destination node and multiple secondary destination nodes via multiple cognitive relay nodes with dynamic spectrum access. The proposed DSTFBC is designed to achieve spatial diversity gain as well as allow for low-complexity decoupling detection at the receiver. Pairwise error probability is then analysed to study the achievable diversity gain of the proposed DSTFBC for different channel models including Rician fading and mixed Rayleigh-Rician fading.

I. Introduction

The demand for spectrum resources in various wireless applications and services is increasing as a result of the rapid development of high data-rate wireless devices. Cognitive radio (CR) has been proposed as an emerging technology to improve spectrum efficiency by efficiently exploiting the underutilised licensed spectrum [1], [2], e.g., secondary users (SUs) are permitted to opportunistically utilise the unused spectrum bands allocated to licensed primary users (PUs).

Multiple-input multiple-output (MIMO) technology is the deployment of multiple antennas at both the source and destination nodes [3]. The MIMO techniques offer significant increases in data throughput and link range without additional bandwidth or transmit power. However, the installation of multiple antennas in mobile handsets restricts the use of MIMO in practice, e.g. for the uplink transmission in cellular networks. Fortunately, mobile users can cooperate to form a virtual multi-antenna system, which can be regarded as a distributed MIMO system. Distributed

Q.-T. Vien, H. X. Nguyen and O. Gemikonakli are with the School of Science and Technology, Middlesex University, The Burroughs, London NW4 4BT, UK. Email: {q.vien; h.nguyen; o.gemikonakli}@mdx.ac.uk.

B. G. Stewart is with the School of Engineering and Built Environment, Glasgow Caledonian University, Cowcaddens Road, Glasgow G4 0BA, UK. Email: b.stewart@gcu.ac.uk.

space-time block codes (DSTBCs) were first introduced in [4] for cooperative communications as a distributed implementation of conventional space-time block codes (STBCs) [5], which were designed for MIMO systems. Initially, DSTBCs were proposed for flat fading channels [4], [6]. The designs of DSTBC in frequency-selective fading channels were then investigated in [7], [8], where a distributed space-time-frequency block code (DSTFBC) was proposed in [7] to achieve spatial and multipath diversity gain and a high-rate DSTFBC was designed in [8] for OFDM systems.

Recently, cooperative diversity has been incorporated into CR networks to construct a cognitive wireless relay network (CWRN) for seamless transmission by exploiting some portions of the spectrum not utilized by the PUs over a period of time [9]. Most of the work on cooperative diversity for CWRNs has considered the transmission of either the PU or the SU over frequency-nonselective fading channels for low data-rate communications (e.g. [9]–[11]). However, in broadband communication standards where the system is required to operate at a high data rate, multipath fading channels become frequency selective. These channels cause severe attenuation in signal strength and unreliable signal detection due to significant inter-symbol interference. In these environments, the cooperative transmission of both the PUs and SUs in a cognitive wireless broadband relay network (CWBRN) has not previously been investigated. In addition, the diversity gain of cooperative communications in an CWBRN for a general frequency-selective fading scenario has also left unevaluated with respect to different locations of the cognitive relays.

To provide a solution to these problems, in this paper, we design a new DSTFBC for two-hop CWBRNs using active cognitive relay nodes which employ the amplify-and-forward (AF) protocol[1]. Single-carrier frequency domain equalisation (SC-FDE) [12] is applied to cope with the multipath fading channels. As illustrated in Fig. 1, the data transmission between PUs and between SUs in an CR network can be realised either with or without the assistance of the other nodes. This stimulates us to consider a two-relay CWBRN as a specific model of multi-relay-based communications[2]. In order to facilitate the simultaneous data transmissions of all the PUs and SUs, spectrum access is firstly investigated in this work to allocate the available frequency bands for the SUs. Specifically, a dynamic spectrum allocation scheme is designed to allocate all the available spectrums to all the SUs in the CWBRNs. In our proposed DSTFBC, the cognitive relays help PU and SUs in the coverage of an CWBRN to transmit their own data to their interested destinations. The main contributions of this paper can be summarised as follows:

[1]The AF relaying protocol is shown to be the best option for cooperative communications to achieve the maximum diversity gain [13].

[2]The considered model is extendible to a multi-relay CWBRN with more than two cognitive relays by changing the operations performed at the cognitive relays to adapt to various network configurations.

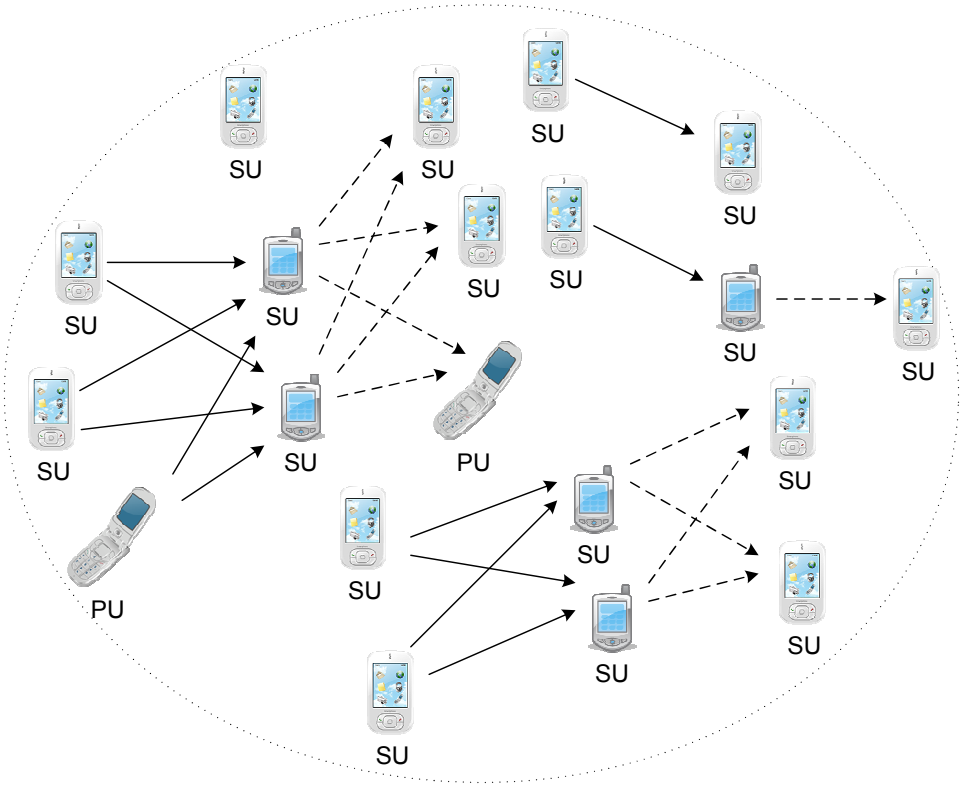

Fig. 1. Cognitive wireless network model.

- A precoding matrix is designed at the cognitive relays such that decoupling detection of desired data blocks in both the time and frequency domains is possible at all destination nodes. This design facilitates the cooperative transmission of both the PU and SUs over frequency-selective fading channels in the CWBRN context.
- Pairwise error probability (PEP) is analysed to study the achievable diversity gain of the proposed DSTFBC for a general scenario where the cognitive relays are located near either the sources or the destinations (i.e., channels are considered a mix of Rayleigh and Rician fading), or where the relays are at the centre of the network (i.e., channels are Rician).
- The derived theoretical results demonstrate that the transmission between the sources and destinations achieves a spatial diversity order of $\min(L_{\mathcal{A}\mathcal{R}_1}, L_{\mathcal{R}_1\mathcal{B}}) + \min(L_{\mathcal{A}\mathcal{R}_2}, L_{\mathcal{R}_2\mathcal{B}})$ if we are using two relay nodes $\mathcal{R}_1$ and $\mathcal{R}_2$ to assist the transmission. Here, $\mathcal{A}$ and $\mathcal{B}$ are a source node and a destination node, respectively. $L_{\mathcal{A}\mathcal{R}_j}$ and $L_{\mathcal{R}_j\mathcal{B}}$, $j = 1, 2$, are the channel memory lengths for the links from $\mathcal{A}$ to $\mathcal{R}_j$ and from $\mathcal{R}_j$ to $\mathcal{B}$, respectively. The analysis also shows that the Rician fading factor in the LOS component provides a coding gain to the PEP performance. This means that, as the fading factor increases, an improved performance is

observed. Additionally, through simulation results, our proposed DSTFBC scheme achieves a lower bit-error-rate (BER) when compared with the conventional interference cancellation scheme, resulting as a consequence of the achievable diversity gain of the proposed DSTFBC scheme.

Notation: Bold lower and upper case letters represent vectors and matrices, respectively. Other notation used in the paper is as follows:

$(\cdot)^T$; $(\cdot)^*$; $(\cdot)^{\mathcal{H}}$	transpose; complex conjugate and Hermitian transpose
$E(\cdot)$; $\Phi(\cdot)$; $f(\cdot)$	expectation value; moment generating and probability density functions
$[\mathbf{x}]_i$; $[\mathbf{A}]_{i,j}$	i-th entry of vector $\mathbf{x}$ and (i,j)-th entry of matrix $\mathbf{A}$
$\|\mathbf{x}\|$	Euclidean norm of vector $\mathbf{x}$
$\mathbf{B} = <\mathbf{A}>^2$	$\mathbf{B} = \mathbf{A}\mathbf{A}^{\mathcal{H}}$
$\mathbf{B} = \mathbf{A}^{1/2}$	a matrix $\mathbf{B}$ such that $\mathbf{B}^2 = \mathbf{A}$
$\otimes$; $\oplus$	matrix direct product and direct sum
$\mathbf{F}_M$	normalised $M \times M$ discrete Fourier transform (DFT) matrix
$\mathbf{0}_{M\times N}$; $\mathbf{I}_N$	zero matrix of size $M \times N$ and identity matrix of size $N \times N$.

II. System Model, Spectrum Allocation and Fading Channel Model

We will discuss system/channel model and spectrum allocation algorithm in this section.

A. System Model and Spectrum Allocation in CWBRN

Fig. 1 illustrates the general system model of the CWBRN consisting of 2 PUs and N_s SUs. An overlay CWBRN is considered where the data transmissions of the PUs are at a higher priority. We assume there are K non-overlapping licensed frequency bands f_1, f_2, $\ldots$, f_K, in a broadband channel. The two PUs can use either the whole or part of the broadband channel to transmit data. Each SU transceiver is equipped with a software defined radio system to tune to any of the K licensed frequency band. The spectrum sensing process at an SU can be carried out using various spectrum sensing techniques (e.g. [14]–[16]). A spectrum indicator vector (SIV) $\boldsymbol{\phi}_i$, $i = 1, 2, \ldots, N_s$, of length K (in bits) is used at the i-th SU to report the availability of frequency bands where bits '0' and '1' represent the frequency band being utilised by the PUs or available, respectively [16]. For example, following an energy detection rule for unknown signals over fading channels [17], the i-th SU, $i = 1, 2, \ldots, N_s$, can detect the usage of the k-th frequency band, $k = 1, 2, \ldots, K$, (i.e. $[\boldsymbol{\phi}_i]_k$) by comparing the energy of the received sensing

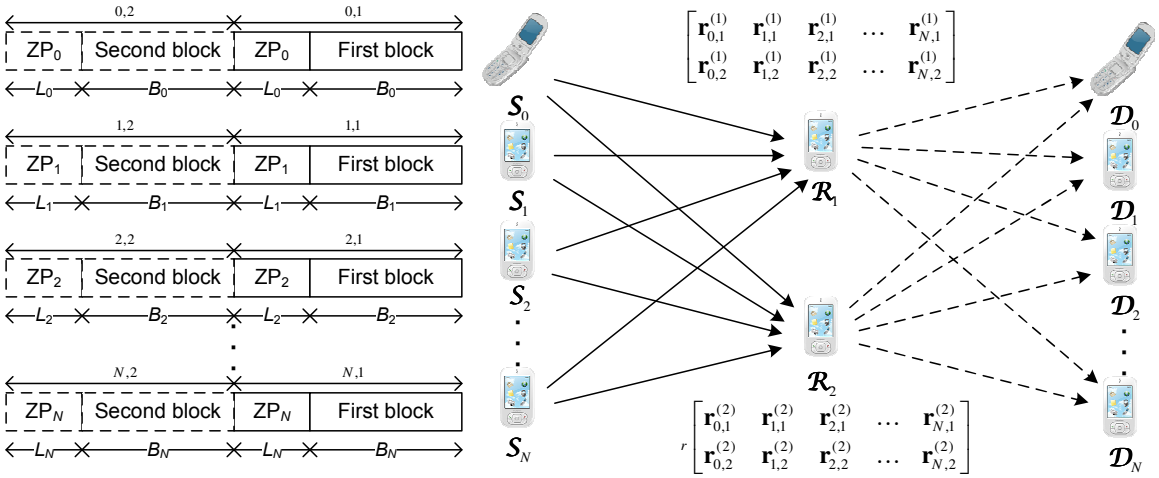

Fig. 2. System model and data transmission in cognitive wireless relay network with the assistance of two cognitive relays.

signal at the k-th frequency band with a corresponding energy threshold. Accordingly, all SIVs at N_s SUs can be written in a spectrum indicator matrix (SIM) form as

$$\mathbf{\Phi} = \left[\boldsymbol{\phi}_1, \boldsymbol{\phi}_2, \ldots, \boldsymbol{\phi}_{N_s}\right]^T, \tag{1}$$

where $[\mathbf{\Phi}]_{i,k}$, $i = 1, 2, \ldots, N_s$, $k = 1, 2, \ldots, K$, represents the availability of the k-th frequency band for the i-th SU. It can be seen that the number of SUs that can communicate depends on the number of frequencies that are occupied by the two PUs. Within CR framework, it is often considered that the states of available frequency can be modelled as a Markov chain where they evolve over time between idle and busy states [18]. However, within the scope of this work, we consider a specific sensing window where we can assume that there are N frequencies ($0 < N < K$) available for the N_s SUs. This means that there are a maximum of N pairs of SUs can communicate with each other using N available frequencies. Therefore, as shown in Fig. 2, we investigate a specific two-relay CWBRN with 1 PU source $\mathcal{S}_0$, 1 PU destination $\mathcal{D}_0$, N SU sources $\{\mathcal{S}_1, \mathcal{S}_2, \ldots, \mathcal{S}_N\}$, 2 SU relays $\{\mathcal{R}_1, \mathcal{R}_2\}$ and N SU destinations $\{\mathcal{D}_1, \mathcal{D}_2, \ldots, \mathcal{D}_N\}$. A half-duplex system is considered where all nodes can either transmit or receive data, but not concurrently. It is assumed that there are no direct links between any pair of source and destination nodes due to either power limitations in each node or distance between nodes or obstacles between nodes. The licensed band for the PU source and PU destination is assumed to be in the range $F_p = \{f_{p_1}, f_{p_2}, \ldots\} \in \{f_1, f_2, \ldots, f_K\}$. From (1), we can allocate the available frequency band $f_{s_i} \in F_s = \{f_1, f_2, \ldots, f_K\} \backslash F_p$, $i = 1, 2, \ldots, N$, for the i-th SU source and i-th SU destination based on the SIM. Here, the operation $\backslash$ in $A \backslash B$ denotes relative complement of set B in set A. The algorithm for this spectrum allocation is summarised in Table I. For clarity,

TABLE I

SPECTRUM ALLOCATION FOR SUS

Step 1. Determine SIV $\boldsymbol{\phi}_i$, $i = 1, 2, \ldots, N_s$, at the i-th SU.
Step 2. Group all SIVs into an SIM (see (1)).
Step 3. Given F_p, select the column index in the SIM corresponding to the available frequency bands for SUs.
Step 4. Group the selected columns in Step 3 into a new matrix, namely free-spectrum indicator matrix (FSIM) $\boldsymbol{\Phi}_0$, where its rows and columns represent available frequency bands and SUs, respectively.
Step 5. Choose sequentially a frequency band for each pair of SUs satisfying this frequency is available for both SUs and is not allocated to other SUs.

let us consider an example of an CWBRN as follows:

Example 1: Let an CWBRN consisting of 2 PUs and 8 SUs (i.e. $N_s = 8$). Suppose that there are 6 non-overlapping frequency bands (i.e. $K = 6$) $\{f_1, f_2, f_3, f_4, f_5, f_6\}$ and 2 PUs occupy f_1 and f_4 for their communications. In this example, we assume the data transmissions expected from SUs include: $\text{SU}_1 \rightarrow \text{SU}_2$, $\text{SU}_3 \rightarrow \text{SU}_4$, $\text{SU}_5 \rightarrow \text{SU}_6$ and $\text{SU}_7 \rightarrow \text{SU}_8$. The SIVs at the 8 SUs are assumed as follows: $\boldsymbol{\phi}_1 = [0,1,0,0,1,1]^T$, $\boldsymbol{\phi}_2 = [0,1,1,0,0,1]^T$, $\boldsymbol{\phi}_3 = [0,0,0,0,1,0]^T$, $\boldsymbol{\phi}_4 = [0,0,1,0,1,0]^T$, $\boldsymbol{\phi}_5 = [0,0,1,0,1,1]^T$, $\boldsymbol{\phi}_6 = [0,1,1,0,0,0]^T$, $\boldsymbol{\phi}_7 = [0,1,0,0,0,0]^T$, $\boldsymbol{\phi}_8 = [0,0,1,0,0,0]^T$. Accordingly, from (1), an SIM is generated as

$$\boldsymbol{\Phi} = \begin{bmatrix} 0 & 1 & 0 & 0 & 1 & 1 \\ 0 & 1 & 1 & 0 & 0 & 1 \\ 0 & 0 & 0 & 0 & 1 & 0 \\ 0 & 0 & 1 & 0 & 1 & 0 \\ 0 & 0 & 1 & 0 & 1 & 1 \\ 0 & 1 & 1 & 0 & 0 & 0 \\ 0 & 1 & 0 & 0 & 0 & 0 \\ 0 & 0 & 1 & 0 & 0 & 0 \end{bmatrix}$$

Since the 2 PUs occupy f_1 and f_4, the available frequency bands for the SUs are f_2, f_3, f_5 and f_6. Based on the above SIM, we can model the allocation of f_2, f_3, f_5 and f_6 to the 8 SUs with

an FSIM as

$$\mathbf{\Phi}_0 = \begin{bmatrix} (f_2) & 1 & 1 & 0 & 0 & 0 & 1 & 1 & 0 \\ (f_3) & 0 & 1 & 0 & 1 & 1 & 1 & 0 & 1 \\ (f_5) & 1 & 0 & 1 & 1 & 1 & 0 & 0 & 0 \\ (f_6) & 1 & 1 & 0 & 0 & 1 & 0 & 0 & 0 \\ & (\text{SU}_1) & (\text{SU}_2) & (\text{SU}_3) & (\text{SU}_4) & (\text{SU}_5) & (\text{SU}_6) & (\text{SU}_7) & (\text{SU}_8) \end{bmatrix},$$

where the row and column indexes correspond the available frequency bands (i.e. f_2, f_3, f_5 and f_6) and the 8 SUs, respectively. Based on the FSIM $\mathbf{\Phi}_0$, we can allocate the frequency bands for the SUs as follows: the communication link $\text{SU}_1 \rightarrow \text{SU}_2$ can be realised using either f_2 or f_6. The frequency bands f_5 and f_3 will be allocated to the communication links $\text{SU}_3 \rightarrow \text{SU}_4$ and $\text{SU}_5 \rightarrow \text{SU}_6$, respectively. The data transmission $\text{SU}_7 \rightarrow \text{SU}_8$ can not be carried out since they sense different available frequency bands. This means that 3 pairs of SUs (i.e. $N = 3$) can simultaneously communicate with each other at the same time with the PUs.

B. Fading Channel Model in CWBRN

In this paper, we take into consideration two typical fading models which include long-term and short-term fading. In wireless communications, long-term fading is caused by path loss and shadowing effects on the data transmission from source node to destination node, while short-term fading characterises the frequency selectivity of the wireless channel between two nodes. Specifically, we characterise long-term and short-term fading between two nodes $\mathcal{A}$ and $\mathcal{B}$, $\{\mathcal{A}, \mathcal{B}\} \in \{\mathcal{S}_0, \mathcal{S}_1, \mathcal{S}_2, \ldots, \mathcal{S}_N, \mathcal{D}_0, \mathcal{D}_1, \mathcal{D}_2, \ldots, \mathcal{D}_N, \mathcal{R}_1, \mathcal{R}_2\}$, by $\xi_{\mathcal{AB}}$ and $\mathbf{h}_{\mathcal{AB}}$, respectively. Here, $\mathbf{h}_{\mathcal{AB}} = [h_{\mathcal{AB}}(1), h_{\mathcal{AB}}(2), \ldots, h_{\mathcal{AB}}(L_{\mathcal{AB}})]^T$, where $L_{\mathcal{AB}}$ is the number of resolvable paths[3] and $h_{\mathcal{AB}}(l)$, $l = 1, 2, \ldots, L_{\mathcal{AB}}$, follows Rician or Nakagami-n distribution having the ratio between the power of the direct component and the average power of the scattered component represented by $n^2_{\mathcal{AB}}(l)$ [19]. Note that Rayleigh fading channel is a special case of Rician fading as $n_{\mathcal{AB}}(l) = 0$. The fading coefficients of the communication channel between two nodes are assumed to be constant over at least two consecutive time slots and vary independently in the next two time slots (i.e. a block fading or quasi-static channel model). The total power gain for each link is normalised to unity, i.e. $E[\|\mathbf{h}_{\mathcal{AB}}\|^2] = 1$.

III. Proposed DSTFBC for CWBRNs and Proof of Decoupling Capability

In this section, we first introduce our proposed DSTFBC for CWBRNs. We then prove that the proposed DSTFBC allows decoupling detection of two data blocks at each destination node in both time and frequency domains.

[3]The proposed DSTFBC can be straightforwardly applied for flat fading channels by setting $L_{\mathcal{AB}} = 1$.

A. Proposed DSTFBC

In Fig. 2, we summarise the structure of transmitted data blocks at $\{\mathcal{S}_0, \mathcal{S}_1, \mathcal{S}_2, \ldots, \mathcal{S}_N\}$. Each source node transmits two information-bearing data blocks to its interested destination through the assistance of two cognitive relay nodes. Each transmitted data block $\mathbf{x}_{i,k}$, $i = 0, 1, 2, \ldots, N$, $k = 1, 2$, of length M_i is generated at $\mathcal{S}_i$ by adding a zero-padding (ZP) sequence ZP_i of length L_i to modulated information data block $\mathbf{s}_{i,k}$ of length B_i, which can be expressed as $\mathbf{x}_{i,k} = \left[\mathbf{s}_{i,k}^T, \mathbf{0}_{1\times L_i}\right]^T$ where $\mathbf{s}_{i,k} = \left[[\mathbf{s}_{i,k}]_1, [\mathbf{s}_{i,k}]_2, \ldots, [\mathbf{s}_{i,k}]_{B_i}\right]^T$. Here, it is noted that various modulation schemes can be applied to the proposed DSTFBC for the CWBRN over frequency selective fading channels. To guarantee that the channel matrices of links $\mathcal{S}_i \to \mathcal{R}_1$, $\mathcal{S}_i \to \mathcal{R}_2$, $\mathcal{R}_1 \to \mathcal{D}_i$ and $\mathcal{R}_2 \to \mathcal{D}_i$ are circulant, the length of ZP_i must satisfy $L_i \geqslant \max(L_{\mathcal{S}_i\mathcal{R}_1} + L_{\mathcal{R}_1\mathcal{D}_i}, L_{\mathcal{S}_i\mathcal{R}_2} + L_{\mathcal{R}_2\mathcal{D}_i})$.

With proper allocation of available frequency bands $\{f_{s_1}, f_{s_2}, \ldots, f_{s_N}\}$ for all SU source and destination nodes (see (1)), $\{\mathcal{S}_0, \mathcal{S}_1, \mathcal{S}_2, \ldots, \mathcal{S}_N\}$ simultaneously transmit two data blocks to both $\mathcal{R}_1$ and $\mathcal{R}_2$ in the first two time slots[4]. $\mathcal{R}_1$ then amplifies and forwards its $(2N+2)$ received signals to the destinations while $\mathcal{R}_2$ precodes its received signals by a precoding matrix before transmitting to all $\{\mathcal{D}_0, \mathcal{D}_1, \mathcal{D}_2, \ldots, \mathcal{D}_N\}$. The idea behind our design is that the precoding at $\mathcal{R}_2$ helps enable the decoupling detection of two desired data blocks at every destination.

Data transmission and precoding process: In the first two time slots, $\mathcal{S}_i$, $i = 0, 1, 2, \ldots, N$, serially transmits $\mathbf{x}_{i,k}$, $k = 1, 2$, to both $\mathcal{R}_1$ and $\mathcal{R}_2$ using its allocated frequency band f_i. The received signal at $\mathcal{R}_j$, $j = 1, 2$, from $\mathcal{S}_i$ is given by

$$\mathbf{r}_{i,k}^{(\mathcal{R}_j)} = \sqrt{\xi_{\mathcal{S}_i\mathcal{R}_j}}\mathbf{H}_{\mathcal{S}_i\mathcal{R}_j}\mathbf{x}_{i,k} + \boldsymbol{\eta}_{i,k}^{(\mathcal{R}_j)}, \tag{2}$$

where $\mathbf{H}_{\mathcal{S}_i\mathcal{R}_j}$ is an $M_i \times M_i$ circulant channel matrix and $\boldsymbol{\eta}_{i,k}^{(\mathcal{R}_j)}$ is a white Gaussian noise vector at $\mathcal{R}_j$ with each entry having zero-mean and variance of $N_0/2$ per dimension. It is noted that for any $M_{\mathcal{AB}} \times M_{\mathcal{AB}}$ circulant matrix $\mathbf{H}_{\mathcal{AB}}$, its (k, l)-th entry is written as $[\mathbf{H}_{\mathcal{AB}}]_{k,l} = [\mathbf{h}_{\mathcal{AB}}]_{((k-l+1) \bmod M_{\mathcal{AB}})}$. From (2), we can rewrite the received signals at $\mathcal{R}_j$, $j = 1, 2$, in vector-matrix form as

$$\mathbf{R}^{(\mathcal{R}_j)} = \begin{bmatrix} \mathbf{r}_{0,1}^{'(\mathcal{R}_j)} & \mathbf{r}_{1,1}^{'(\mathcal{R}_j)} & \mathbf{r}_{2,1}^{'(\mathcal{R}_j)} & \cdots & \mathbf{r}_{N,1}^{'(\mathcal{R}_j)} \\ \mathbf{r}_{0,2}^{'(\mathcal{R}_j)} & \mathbf{r}_{1,2}^{'(\mathcal{R}_j)} & \mathbf{r}_{2,2}^{'(\mathcal{R}_j)} & \cdots & \mathbf{r}_{N,2}^{'(\mathcal{R}_j)} \end{bmatrix}, \tag{3}$$

where $\mathbf{r}_{i,k}^{'(\mathcal{R}_j)}$, $i = 0, 1, 2, \ldots, N$, $k = 1, 2$, is a zero-padded signal after adding ZP sequences to the received signal $\mathbf{r}_{i,k}^{(\mathcal{R}_j)}$ to match the length of $M = \max(M_0, M_1, \ldots, M_N)$. Thus, the size of matrix $\mathbf{R}^{(\mathcal{R}_j)}$ is $2M \times (N + 1)$.

[4]A time slot is defined as the time to transmit a block of symbols.

What is novel in the proposed DSTFBC is that the received signal at $\mathcal{R}_2$ is conjugated and then precoded by a precoding matrix $\mathbf{P_R}$ defined as follows:

$$\mathbf{P_R} = \begin{bmatrix} \mathbf{0}_{M\times M} & -\mathbf{P}_M^{(G)} \\ \mathbf{P}_M^{(G)} & \mathbf{0}_{M\times M} \end{bmatrix}, \tag{4}$$

where the matrix $\mathbf{P}_M^{(G)}$ is designed as

$$\mathbf{P}_M^{(G)} = \begin{bmatrix} \mathbf{P}_1 & \mathbf{0}_{G\times(M-G)} \\ \mathbf{0}_{(M-G)\times G} & \mathbf{P}_2 \end{bmatrix} = \mathbf{P}_1 \oplus \mathbf{P}_2. \tag{5}$$

In (5), the matrix $\mathbf{P}_1$ of size $G\times G$ and the matrix $\mathbf{P}_2$ of size $(M-G)\times(M-G)$ have (l,k)-th elements given by

$$[\mathbf{P}_1]_{l,k} = \begin{cases} 1 & \text{if } k = G-l+1, \\ 0 & \text{otherwise,} \end{cases} \tag{6}$$

$$[\mathbf{P}_2]_{l,k} = \begin{cases} 1 & \text{if } k = M-G-l+1, \\ 0 & \text{otherwise.} \end{cases} \tag{7}$$

In order to ensure that, after precoding, at least the last $L_{\mathcal{S}_i\mathcal{R}_2}$, $i = 0, 1, 2, \ldots, N$, samples of $-\mathbf{P}_M^{(G)}\mathbf{r}_{i,2}^{'(\mathcal{R}_2)}$ and $\mathbf{P}_M^{(G)}\mathbf{r}_{i,1}^{'(\mathcal{R}_2)}$ are all zeros to make the channel matrix $\mathcal{R}_2 \to \mathcal{D}_i$ circulant, we choose $G = \max(B_0, B_1, B_2, \ldots, B_N) + \max(L_{\mathcal{S}_0\mathcal{R}_2}, L_{\mathcal{S}_1\mathcal{R}_2}, L_{\mathcal{S}_2\mathcal{R}_2}, \ldots, L_{\mathcal{S}_N\mathcal{R}_2})$. The proposed DSTFBC is specifically designed at the data-block level to assist the cooperative data transmission of the PU and SUs in CWBRNs via two cognitive relay nodes.

Subsequently, each cognitive relay $\mathcal{R}_j$, $j = 1, 2$, normalises its received signal $\mathbf{r}_{i,k}^{(\mathcal{R}_j)}$, $i = 0, 1, 2, \ldots, N$, $k = 1, 2$, in (2) by a factor $\alpha_i^{(\mathcal{R}_j)} = \sqrt{E\left[\left\|\mathbf{r}_{i,k}^{(\mathcal{R}_j)}\right\|^2\right]} = \sqrt{\xi_{\mathcal{S}_i\mathcal{R}_j} + N_0}$ to have unit average energy. Thus, the transmitted signals from $\mathcal{R}_j$, $j = 1, 2$, can be written by

$$\mathbf{X}^{(\mathcal{R}_1)} = \mathbf{R}_0^{(\mathcal{R}_1)}, \tag{8}$$

$$\mathbf{X}^{(\mathcal{R}_2)} = \mathbf{P_R}\left[\mathbf{R}_0^{(\mathcal{R}_2)}\right]^*, \tag{9}$$

where $\mathbf{R}_0^{(\mathcal{R}_j)}$ is the normalised received signal at $\mathcal{R}_j$, which is given by

$$\mathbf{R}_0^{(\mathcal{R}_j)} = \begin{bmatrix} \frac{1}{\alpha_0^{(\mathcal{R}_j)}}\mathbf{r}_{0,1}^{'(\mathcal{R}_j)} & \frac{1}{\alpha_1^{(\mathcal{R}_j)}}\mathbf{r}_{1,1}^{'(\mathcal{R}_j)} & \frac{1}{\alpha_2^{(\mathcal{R}_j)}}\mathbf{r}_{2,1}^{'(\mathcal{R}_j)} & \cdots & \frac{1}{\alpha_N^{(\mathcal{R}_j)}}\mathbf{r}_{N,1}^{'(\mathcal{R}_j)} \\ \frac{1}{\alpha_0^{(\mathcal{R}_j)}}\mathbf{r}_{0,2}^{'(\mathcal{R}_j)} & \frac{1}{\alpha_1^{(\mathcal{R}_j)}}\mathbf{r}_{1,2}^{'(\mathcal{R}_j)} & \frac{1}{\alpha_2^{(\mathcal{R}_j)}}\mathbf{r}_{2,2}^{'(\mathcal{R}_j)} & \cdots & \frac{1}{\alpha_N^{(\mathcal{R}_j)}}\mathbf{r}_{N,2}^{'(\mathcal{R}_j)} \end{bmatrix}. \tag{10}$$

Following precoding, $\mathcal{R}_1$ and $\mathcal{R}_2$ simultaneously forward their messages to $\{\mathcal{D}_0, \mathcal{D}_1, \mathcal{D}_2, \ldots, \mathcal{D}_N\}$ using $\{F_p, f_{s_1}, f_{s_2}, \ldots, f_{s_N}\}$ in the subsequent $(2N+2)$ time slots. The received signals at $\mathcal{D}_i$, $i = 0, 1, 2, \ldots, N$, are

$$\mathbf{r}_1^{(\mathcal{D}_i)} = \sqrt{\xi_{\mathcal{R}_1\mathcal{D}_i}}\mathbf{H}_{\mathcal{R}_1\mathcal{D}_i}\frac{1}{\alpha_i^{(\mathcal{R}_1)}}\mathbf{r}_{i,1}^{'(\mathcal{R}_1)} - \sqrt{\xi_{\mathcal{R}_2\mathcal{D}_i}}\mathbf{H}_{\mathcal{R}_2\mathcal{D}_i}\frac{1}{\alpha_i^{(\mathcal{R}_2)}}\mathbf{P}_M^{(G)}\left[\mathbf{r}_{i,2}^{'(\mathcal{R}_2)}\right]^* + \boldsymbol{\eta}_1^{(\mathcal{D}_i)}, \tag{11}$$

$$\mathbf{r}_2^{(\mathcal{D}_i)} = \sqrt{\xi_{\mathcal{R}_1\mathcal{D}_i}}\mathbf{H}_{\mathcal{R}_1\mathcal{D}_i}\frac{1}{\alpha_i^{(\mathcal{R}_1)}}\mathbf{r}_{i,2}^{\prime(\mathcal{R}_1)} + \sqrt{\xi_{\mathcal{R}_2\mathcal{D}_i}}\mathbf{H}_{\mathcal{R}_2\mathcal{D}_i}\frac{1}{\alpha_i^{(\mathcal{R}_2)}}\mathbf{P}_M^{(G)}\left[\mathbf{r}_{i,1}^{\prime(\mathcal{R}_2)}\right]^* + \boldsymbol{\eta}_2^{(\mathcal{D}_i)}, \quad (12)$$

where $\mathbf{H}_{\mathcal{R}_j\mathcal{D}_i}$, $j = 1, 2$, is an $M \times M$ circulant channel matrix and $\boldsymbol{\eta}_k^{(\mathcal{D}_i)}$, $k = 1, 2$, is a white Gaussian noise vector at $\mathcal{D}_i$ with each entry having zero-mean and variance of $N_0/2$ per dimension.

Substituting (2) into (11) and (12), we obtain

$$\mathbf{r}_1^{(\mathcal{D}_i)} = \sqrt{\frac{\xi_{\mathcal{S}_i\mathcal{R}_1}\xi_{\mathcal{R}_1\mathcal{D}_i}}{\xi_{\mathcal{S}_i\mathcal{R}_1} + N_0}}\mathbf{H}_{\mathcal{R}_1\mathcal{D}_i}\mathbf{H}_{\mathcal{S}_i\mathcal{R}_1}\mathbf{x}_{i,1} - \sqrt{\frac{\xi_{\mathcal{S}_i\mathcal{R}_2}\xi_{\mathcal{R}_2\mathcal{D}_i}}{\xi_{\mathcal{S}_i\mathcal{R}_2} + N_0}}\mathbf{H}_{\mathcal{R}_2\mathcal{D}_i}\mathbf{P}_M^{(G)}\mathbf{H}_{\mathcal{S}_i\mathcal{R}_2}^*\mathbf{x}_{i,2}^* + \boldsymbol{\eta}_1^{\prime(\mathcal{D}_i)}, \quad (13)$$

$$\mathbf{r}_2^{(\mathcal{D}_i)} = \sqrt{\frac{\xi_{\mathcal{S}_i\mathcal{R}_1}\xi_{\mathcal{R}_1\mathcal{D}_i}}{\xi_{\mathcal{S}_i\mathcal{R}_1} + N_0}}\mathbf{H}_{\mathcal{R}_1\mathcal{D}_i}\mathbf{H}_{\mathcal{S}_i\mathcal{R}_1}\mathbf{x}_{i,2} + \sqrt{\frac{\xi_{\mathcal{S}_i\mathcal{R}_2}\xi_{\mathcal{R}_2\mathcal{D}_i}}{\xi_{\mathcal{S}_i\mathcal{R}_2} + N_0}}\mathbf{H}_{\mathcal{R}_2\mathcal{D}_i}\mathbf{P}_M^{(G)}\mathbf{H}_{\mathcal{S}_i\mathcal{R}_2}^*\mathbf{x}_{s_i,1}^* + \boldsymbol{\eta}_2^{\prime(\mathcal{D}_i)}, \quad (14)$$

where $\boldsymbol{\eta}_k^{\prime(\mathcal{D}_i)}$, $k = 1, 2$, $i = 0, 1, 2, \ldots, N$, is an effective noise term including Gaussian noise at both cognitive relays and destination. It can be seen that the received signals given by (13) and (14) consist of both data blocks, which therefore introduces interference at the destination nodes. In order to detect each data block separately for the best performance, the data blocks require to be decoupled.

B. Decoupling in Time and Frequency Domains

For the sake of a fair comparison with other systems, we firstly normalise the noise variance of the received signals at $\mathcal{D}_i$, $i = 0, 1, 2, \ldots, N$, to be N_0 prior to implementing data detection. Thus, we normalise the received signals at $\mathcal{D}_i$ by a factor

$$\alpha^{(\mathcal{D}_i)} = \sqrt{\frac{\xi_{\mathcal{R}_1\mathcal{D}_i}}{\xi_{\mathcal{S}_i\mathcal{R}_1} + N_0}\sum_{l=1}^{L_{\mathcal{R}_1\mathcal{D}_i}}\left|[\mathbf{h}_{\mathcal{R}_1\mathcal{D}_i}]_l\right|^2 + \frac{\xi_{\mathcal{R}_2\mathcal{D}_i}}{\xi_{\mathcal{S}_i\mathcal{R}_2} + N_0}\sum_{l=1}^{L_{\mathcal{R}_2\mathcal{D}_i}}\left|[\mathbf{h}_{\mathcal{R}_2\mathcal{D}_i}]_l\right|^2 + 1}. \quad (15)$$

Accordingly, the normalised signals at $\mathcal{D}_i$ can be written as

$$\mathbf{r}_1^{\prime(\mathcal{D}_i)} = \frac{1}{\alpha^{(\mathcal{D}_i)}}\mathbf{r}_1^{(\mathcal{D}_i)} = \alpha_{i,1}\mathbf{H}_{\mathcal{R}_1\mathcal{D}_i}\mathbf{H}_{\mathcal{S}_i\mathcal{R}_1}\mathbf{x}_{i,1} - \alpha_{i,2}\mathbf{H}_{\mathcal{R}_2\mathcal{D}_i}\mathbf{P}_M^{(G)}\mathbf{H}_{\mathcal{S}_i\mathcal{R}_2}^*\mathbf{x}_{i,2}^* + \boldsymbol{\eta}_1^{\prime\prime(\mathcal{D}_i)}, \quad (16)$$

$$\mathbf{r}_2^{\prime(\mathcal{D}_i)} = \frac{1}{\alpha^{(\mathcal{D}_i)}}\mathbf{r}_2^{(\mathcal{D}_i)} = \alpha_{i,1}\mathbf{H}_{\mathcal{R}_1\mathcal{D}_i}\mathbf{H}_{\mathcal{S}_i\mathcal{R}_1}\mathbf{x}_{i,2} + \alpha_{i,2}\mathbf{H}_{\mathcal{R}_2\mathcal{D}_i}\mathbf{P}_M^{(G)}\mathbf{H}_{\mathcal{S}_i\mathcal{R}_2}^*\mathbf{x}_{i,1}^* + \boldsymbol{\eta}_2^{\prime\prime(\mathcal{D}_i)}, \quad (17)$$

where $\boldsymbol{\eta}_k^{\prime\prime(\mathcal{D}_i)}$, $k = 1, 2$, is a normalised complex Gaussian noise vector in which each entry has zero mean and variance of $N_0/2$ per dimension. Here, $\alpha_{i,j}$, $j = 1, 2$, $i = 0, 1, 2, \ldots, N$, is defined as

$$\alpha_{i,j} = \sqrt{\frac{\alpha_{i,n\neq j}^{\prime}\alpha_{i,j}^{\prime\prime}\xi_{\mathcal{S}_i\mathcal{R}_j}}{\alpha_{i,1}^{\prime}\alpha_{i,2}^{\prime} + \alpha_{i,2}^{\prime}\alpha_{i,1}^{\prime\prime}\sum_{l=1}^{L_{\mathcal{R}_1\mathcal{D}_i}}\left|[\mathbf{h}_{\mathcal{R}_1\mathcal{D}_i}]_l\right|^2 + \alpha_{i,1}^{\prime}\alpha_{i,2}^{\prime\prime}\sum_{l=1}^{L_{\mathcal{R}_2\mathcal{D}_i}}\left|[\mathbf{h}_{\mathcal{R}_2\mathcal{D}_i}]_l\right|^2}}, \quad (18)$$

where $n \in \{1,2\}$, $\alpha'_{i,j} = 1 + \xi_{\mathcal{S}_i\mathcal{R}_j}/N_0$ and $\alpha''_{i,j} = \xi_{\mathcal{R}_j\mathcal{D}_i}/N_0$.

For the data decoupling process, we conjugate both sides of (17) and then multiply with $\mathbf{P}_M^{(G)}$. Based on the fact that $\mathbf{P}_M^{(G)}\mathbf{H}_{\mathcal{AB}}^{*}\mathbf{P}_M^{(G)} = \mathbf{H}_{\mathcal{AB}}^{\mathcal{H}}$ for any $M \times M$ circulant matrix $\mathbf{H}_{\mathcal{AB}}$, we obtain

$$\mathbf{r}_2^{''(\mathcal{D}_i)} = \alpha_{i,2}\mathbf{H}_{\mathcal{R}_2\mathcal{D}_i}^{\mathcal{H}}\mathbf{H}_{\mathcal{S}_i\mathcal{R}_2}\mathbf{x}_{i,1} + \alpha_{i,1}\mathbf{H}_{\mathcal{R}_1\mathcal{D}_i}^{\mathcal{H}}\mathbf{H}_{\mathcal{S}_i\mathcal{R}_1}^{\mathcal{H}}\mathbf{P}_M^{(G)}\mathbf{x}_{i,2}^{*} + \mathbf{P}_M^{(G)}[\boldsymbol{\eta}_2^{''(\mathcal{D}_i)}]^{*}. \tag{19}$$

From (16) and (19), we can group the equations in vector-matrix forms as

$$\mathbf{R}^{(\mathcal{D}_i)} = \begin{bmatrix} \mathbf{r}_1^{'(\mathcal{D}_i)} \\ \mathbf{r}_2^{''(\mathcal{D}_i)} \end{bmatrix} = \mathbf{H}_i \begin{bmatrix} \mathbf{x}_{i,1} \\ \mathbf{P}_M^{(G)}\mathbf{x}_{i,2}^{*} \end{bmatrix} + \begin{bmatrix} \boldsymbol{\eta}_1^{''(\mathcal{D}_i)} \\ \mathbf{P}_M^{(G)}[\boldsymbol{\eta}_2^{''(\mathcal{D}_i)}]^{*} \end{bmatrix}, \tag{20}$$

where

$$\mathbf{H}_i \triangleq \begin{bmatrix} \alpha_{i,1}\mathbf{H}_{\mathcal{R}_1\mathcal{D}_i}\mathbf{H}_{\mathcal{S}_i\mathcal{R}_1} & -\alpha_{i,2}\mathbf{H}_{\mathcal{R}_2\mathcal{D}_i}\mathbf{H}_{\mathcal{S}_i\mathcal{R}_2}^{\mathcal{H}} \\ \alpha_{i,2}\mathbf{H}_{\mathcal{R}_2\mathcal{D}_i}^{\mathcal{H}}\mathbf{H}_{\mathcal{S}_i\mathcal{R}_2} & \alpha_{i,1}\mathbf{H}_{\mathcal{R}_1\mathcal{D}_i}^{\mathcal{H}}\mathbf{H}_{\mathcal{S}_i\mathcal{R}_1}^{\mathcal{H}} \end{bmatrix}. \tag{21}$$

Let us denote $\boldsymbol{\Omega}_i = [\alpha_{i,1}^2 <\mathbf{H}_{\mathcal{S}_i\mathcal{R}_1}>^2 <\mathbf{H}_{\mathcal{R}_1\mathcal{D}_i}>^2 + \alpha_{i,2}^2 <\mathbf{H}_{\mathcal{S}_i\mathcal{R}_2}>^2 <\mathbf{H}_{\mathcal{R}_2\mathcal{D}_i}>^2]^{\frac{1}{2}}$. Then, $\mathbf{H}_i^{\mathcal{H}}\mathbf{H}_i = \mathbf{I}_2 \otimes \boldsymbol{\Omega}_i^2$, which is a block-diagonal matrix. Thus, we can decouple the detection of two data blocks independently by multiplying both sides of (20) with the unitary matrix $(\mathbf{I}_2 \otimes \boldsymbol{\Omega}_i^{-1})\mathbf{H}_i^{\mathcal{H}}$ as

$$\mathbf{Y}^{(\mathcal{D}_i)} = \begin{bmatrix} \mathbf{y}_1^{(\mathcal{D}_i)} \\ \mathbf{y}_2^{(\mathcal{D}_i)} \end{bmatrix} = (\mathbf{I}_2 \otimes \boldsymbol{\Omega}_i^{-1})\mathbf{H}_i^{\mathcal{H}}\mathbf{R}^{(\mathcal{D}_i)} = \begin{bmatrix} \boldsymbol{\Omega}_i\mathbf{x}_{i,1} \\ \boldsymbol{\Omega}_i\mathbf{P}_M^{(G)}\mathbf{x}_{i,2}^{*} \end{bmatrix} + \begin{bmatrix} \bar{\boldsymbol{\eta}}_1^{(\mathcal{D}_i)} \\ \bar{\boldsymbol{\eta}}_2^{(\mathcal{D}_i)} \end{bmatrix}, \tag{22}$$

where $\bar{\boldsymbol{\eta}}_k^{(\mathcal{D}_i)}$, $k = 1, 2$, is the Gaussian noise vector resulting from the decoupling process with each entry having zero mean and variance of $N_0/2$ per dimension. We have the following observation (OB):

(OB1) Decoupling Capability of Data Blocks: From (22), two data blocks transmitted from $\mathcal{S}_i$, $i = 0, 1, 2, \ldots, N$, can be detected independently at $\mathcal{D}_i$ by using general maximum likelihood (ML) detection in the time domain. However, general ML detection requires high computational complexity that increases exponentially with the channel memory lengths.

Therefore, we now introduce low-complexity decoupling of data blocks using frequency-domain equalisation. It is noted that the circulant matrix $\mathbf{H}_{\mathcal{AB}}$ of size $M \times M$ can be diagonalised as $\mathbf{H}_{\mathcal{AB}} = \mathbf{F}_M^{\mathcal{H}}\boldsymbol{\Lambda}_{\mathcal{AB}}\mathbf{F}_M$ where $\boldsymbol{\Lambda}_{\mathcal{AB}}$ is an $M \times M$ diagonal matrix with diagonal entries created by the M-point DFT of the first column of $\mathbf{H}_{\mathcal{AB}}$. Thus, we can transform (20) into the frequency domain by taking the DFT of both sides of the equation, which results in

$$\mathbf{R}_f^{(\mathcal{D}_i)} = \begin{bmatrix} \mathbf{r}_{f,1}^{(\mathcal{D}_i)} \\ \mathbf{r}_{f,2}^{(\mathcal{D}_i)} \end{bmatrix} = \begin{bmatrix} \mathbf{F}_M\mathbf{r}_1^{'\mathcal{D}_i)} \\ \mathbf{F}_M\mathbf{r}_2^{''\mathcal{D}_i)} \end{bmatrix} = \boldsymbol{\Lambda}_i \begin{bmatrix} \mathbf{F}_M\mathbf{x}_{i,1} \\ \mathbf{F}_M\mathbf{P}_M^{(G)}\mathbf{x}_{i,2}^{*} \end{bmatrix} + \begin{bmatrix} \mathbf{F}_M\boldsymbol{\eta}_1^{''(\mathcal{D}_i)} \\ \mathbf{F}_M\mathbf{P}_M^{(G)}[\boldsymbol{\eta}_2^{''(\mathcal{D}_i)}]^{*} \end{bmatrix}, \tag{23}$$

where

$$\boldsymbol{\Lambda}_i \triangleq \begin{bmatrix} \alpha_{i,1}\boldsymbol{\Lambda}_{\mathcal{R}_1\mathcal{D}_i}\boldsymbol{\Lambda}_{\mathcal{S}_i\mathcal{R}_1} & -\alpha_{i,2}\boldsymbol{\Lambda}_{\mathcal{R}_2\mathcal{D}_i}\boldsymbol{\Lambda}_{\mathcal{S}_i\mathcal{R}_2}^{*} \\ \alpha_{i,2}\boldsymbol{\Lambda}_{\mathcal{R}_2\mathcal{D}_i}^{*}\boldsymbol{\Lambda}_{\mathcal{S}_i\mathcal{R}_2} & \alpha_{i,1}\boldsymbol{\Lambda}_{\mathcal{R}_1\mathcal{D}_i}^{*}\boldsymbol{\Lambda}_{\mathcal{S}_i\mathcal{R}_1}^{*} \end{bmatrix}. \tag{24}$$

Let us denote $\mathbf{\Psi}_i = [\alpha_{i,1}^2 <\mathbf{\Lambda}_{\mathcal{S}_i\mathcal{R}_1}>^2 <\mathbf{\Lambda}_{\mathcal{R}_1\mathcal{D}_i}>^2 + \alpha_{i,2}^2 <\mathbf{\Lambda}_{\mathcal{S}_i\mathcal{R}_2}>^2 <\mathbf{\Lambda}_{\mathcal{R}_2\mathcal{D}_i}>^2]^{\frac{1}{2}}$. We observe that $\mathbf{\Lambda}_i^{\mathcal{H}}\mathbf{\Lambda}_i = \mathbf{I}_2 \otimes \mathbf{\Psi}_i^2$, which is a block-diagonal matrix. Thus, by multiplying both sides of (23) with the unitary matrix $(\mathbf{I}_2 \otimes \mathbf{\Psi}_i^{-1})\mathbf{\Lambda}_i^{\mathcal{H}}$, we can decouple the detection of each data block at $\mathcal{D}_i$, $i = 0, 1, 2, \ldots, N$, in the frequency domain as follows:

$$\mathbf{Y}_f^{(\mathcal{D}_i)} = \begin{bmatrix} \mathbf{y}_{f,1}^{(\mathcal{D}_i)} \\ \mathbf{y}_{f,2}^{(\mathcal{D}_i)} \end{bmatrix} = (\mathbf{I}_2 \otimes \mathbf{\Psi}_{s_i}^{-1})\mathbf{\Lambda}_p^{\mathcal{H}}\mathbf{R}_f^{(\mathcal{S}\mathcal{D}_i)} = \begin{bmatrix} \mathbf{\Psi}_i\mathbf{F}_M\mathbf{x}_{i,1} \\ \mathbf{\Psi}_i\mathbf{F}_M\mathbf{P}_M^{(G)}\mathbf{x}_{i,2}^* \end{bmatrix} + \begin{bmatrix} \bar{\boldsymbol{\eta}}_{f,1}^{(\mathcal{D}_i)} \\ \bar{\boldsymbol{\eta}}_{f,2}^{(\mathcal{D}_i)} \end{bmatrix}, \tag{25}$$

where $\bar{\boldsymbol{\eta}}_{f,k}^{(\mathcal{D}_i)}$, $k = 1, 2$, is the equivalent noise vector for the k-block at $\mathcal{D}_i$ resulting from the decoupling process in the frequency domain. Since $\mathbf{\Psi}_i$ is diagonal, we can decompose (25) into scalar equations as

$$\left[\mathbf{y}_{f,1}^{(\mathcal{D}_i)}\right]_n = [\mathbf{\Psi}_i]_{n,n}\left[\mathbf{F}_M\mathbf{x}_{i,1}\right]_n + \left[\bar{\boldsymbol{\eta}}_{f,1}^{(\mathcal{D}_i)}\right]_n, \tag{26}$$

$$\left[\mathbf{y}_{f,2}^{(\mathcal{D}_i)}\right]_n = [\mathbf{\Psi}_i]_{n,n}\left[\mathbf{F}_M\mathbf{P}_M^{(G)}\mathbf{x}_{i,2}^*\right]_n + \left[\bar{\boldsymbol{\eta}}_{f,2}^{(\mathcal{D}_i)}\right]_n, \tag{27}$$

where $n = 1, 2, \ldots, M$. Thus, we can independently evaluate each of $\left[\mathbf{F}_M\mathbf{x}_{i,1}\right]_n$ and $\left[\mathbf{F}_M\mathbf{P}_M^{(G)}\mathbf{x}_{i,2}^*\right]_n$ using linear equalisation, and then transform the evaluated outputs into the time domain to detect $[\mathbf{x}_{i,k}]_n$, $k = 1, 2$, accordingly.

IV. Performance Analysis

In this section, we derive the PEP expression of the proposed DSTFBC scheme for CWBRNs over frequency selective fading channels. Three typical scenarios are taken into consideration:

(*a*) The cognitive relay nodes are located near the source nodes, i.e. links from $\{\mathcal{S}_0, \mathcal{S}_1, \mathcal{S}_2, \ldots, \mathcal{S}_N\}$ to $\{\mathcal{R}_1, \mathcal{R}_2\}$ experience Rician fading, and those from $\{\mathcal{R}_1, \mathcal{R}_2\}$ to $\{\mathcal{D}_0, \mathcal{D}_1, \mathcal{D}_2, \ldots, \mathcal{D}_N\}$ experience Rayleigh fading.

(*b*) The cognitive relays are located near the centre of the network, i.e. all links from $\{\mathcal{S}_0, \mathcal{S}_1, \mathcal{S}_2, \ldots, \mathcal{S}_N\}$ to $\{\mathcal{R}_1, \mathcal{R}_2\}$ and from $\{\mathcal{R}_1, \mathcal{R}_2\}$ to $\{\mathcal{D}_0, \mathcal{D}_1, \mathcal{D}_2, \ldots, \mathcal{D}_N\}$ experience Rician fading.

(*c*) The cognitive relays are located near the destination nodes, i.e. links from $\{\mathcal{S}_0, \mathcal{S}_1, \mathcal{S}_2, \ldots, \mathcal{S}_N\}$ to $\{\mathcal{R}_1, \mathcal{R}_2\}$ experience Rayleigh fading, and those from $\{\mathcal{R}_1, \mathcal{R}_2\}$ to $\{\mathcal{D}_0, \mathcal{D}_1, \mathcal{D}_2, \ldots, \mathcal{D}_N\}$ experience Rician fading.

It can be seen that the PEP expression for scenario (c) can be obtained simply from scenario (a) with some interchanged parameters. Thus, it is sufficient to analyse the PEP for scenarios (a) and (b).

Let us denote a decoded codeword vector at $\mathcal{D}_i$, $i = 0, 1, 2, \ldots, N$, as $\hat{\mathbf{x}}_i$. The conditional PEP is calculated by

$$P(\mathbf{x}_i \to \hat{\mathbf{x}}_i | \mathbf{h}_{\mathcal{S}_i\mathcal{R}_1}, \mathbf{h}_{\mathcal{S}_i\mathcal{R}_2}, \mathbf{h}_{\mathcal{R}_1\mathcal{D}_i}, \mathbf{h}_{\mathcal{R}_2\mathcal{D}_i}) = Q\left(\sqrt{\frac{d^2(\mathbf{x}_i, \hat{\mathbf{x}}_i)}{2N_0}}\right), \tag{28}$$

where $Q(\cdot)$ is the Q function and $d(\mathbf{x}_i, \hat{\mathbf{x}}_i)$ is the Euclidean distance between $\mathbf{x}_i$ and $\hat{\mathbf{x}}_i$. By applying the Chernoff bound to the Q function [20], the PEP in (28) can be upper bounded by

$$P(\mathbf{x}_i \to \hat{\mathbf{x}}_i | \mathbf{h}_{\mathcal{S}_i\mathcal{R}_1}, \mathbf{h}_{\mathcal{S}\mathcal{R}_2}, \mathbf{h}_{\mathcal{R}_1\mathcal{D}_i}, \mathbf{h}_{\mathcal{R}_2\mathcal{D}_i}) \leqslant \exp\left(-\frac{d^2(\mathbf{x}_i, \hat{\mathbf{x}}_i)}{4N_0}\right). \tag{29}$$

From (20), the Euclidean distance in (29) is calculated by

$$d^2(\mathbf{x}_i, \hat{\mathbf{x}}_i) = \alpha_{i,1}^2 \|\mathbf{H}_{\mathcal{R}_1\mathcal{D}_i}\mathbf{H}_{\mathcal{S}_i\mathcal{R}_1}(\mathbf{x}_{i,1} - \hat{\mathbf{x}}_{i,1})\|^2 + \alpha_{i,2}^2 \|\mathbf{H}_{\mathcal{R}_2\mathcal{D}_i}\mathbf{H}_{\mathcal{S}_i\mathcal{R}_2}\mathbf{P}_M^{(G)}(\mathbf{x}_{i,2} - \hat{\mathbf{x}}_{i,2})\|^2. \tag{30}$$

We can approximate (30) as one of four possible forms as:

$$\begin{aligned} d^2(\mathbf{x}_i, \hat{\mathbf{x}}_i) &\approx \frac{\alpha_{i,1}^2}{M}||\mathbf{H}_{\mathcal{R}_1\mathcal{D}_i}||^2||\mathbf{H}_{\mathcal{S}_i\mathcal{R}_1}\mathbf{e}_1||^2 + \frac{\alpha_{i,2}^2}{M}||\mathbf{H}_{\mathcal{R}_2\mathcal{D}_i}||^2||\mathbf{H}_{\mathcal{S}_i\mathcal{R}_2}\mathbf{e}_2||^2 \\ &\approx \frac{\alpha_{i,1}^2}{M}||\mathbf{H}_{\mathcal{S}_i\mathcal{R}_1}||^2||\mathbf{H}_{\mathcal{R}_1\mathcal{D}_i}\mathbf{e}_1||^2 + \frac{\alpha_{i,2}^2}{M}||\mathbf{H}_{\mathcal{R}_2\mathcal{D}_i}||^2||\mathbf{H}_{\mathcal{S}_i\mathcal{R}_2}\mathbf{e}_2||^2 \\ &\approx \frac{\alpha_{i,1}^2}{M}||\mathbf{H}_{\mathcal{R}_1\mathcal{D}_i}||^2||\mathbf{H}_{\mathcal{S}_i\mathcal{R}_1}\mathbf{e}_1||^2 + \frac{\alpha_{i,2}^2}{M}||\mathbf{H}_{\mathcal{S}_i\mathcal{R}_2}||^2||\mathbf{H}_{\mathcal{R}_2\mathcal{D}_i}\mathbf{e}_2||^2 \\ &\approx \frac{\alpha_{i,1}^2}{M}||\mathbf{H}_{\mathcal{S}_i\mathcal{R}_1}||^2||\mathbf{H}_{\mathcal{R}_1\mathcal{D}_i}\mathbf{e}_1||^2 + \frac{\alpha_{i,2}^2}{M}||\mathbf{H}_{\mathcal{S}_i\mathcal{R}_2}||^2||\mathbf{H}_{\mathcal{R}_2\mathcal{D}_i}\mathbf{e}_2||^2, \end{aligned} \tag{31}$$

where $\mathbf{e}_k = \mathbf{x}_{i,k} - \hat{\mathbf{x}}_{i,k}$, $k = 1, 2$. Note that $||\mathbf{H}_{\mathcal{A}\mathcal{B}}||^2 = M\sum_{l_{\mathcal{A}\mathcal{B}}=1}^{L_{\mathcal{A}\mathcal{B}}} |[\mathbf{h}_{\mathcal{A}\mathcal{B}}]_{l_{\mathcal{A}\mathcal{B}}}|^2$ and $||\mathbf{H}_{\mathcal{A}\mathcal{B}}\mathbf{e}_k||^2 = \sum_{l_{\mathcal{A}\mathcal{B}}=1}^{L_{\mathcal{A}\mathcal{B}}} [\boldsymbol{\lambda}_k]_{l_{\mathcal{A}\mathcal{B}}}|[\boldsymbol{\nu}_k]_{l_{\mathcal{A}\mathcal{B}}}|^2$, $k = 1, 2$, $\mathcal{A}, \mathcal{B} \in \{\mathcal{S}_i, \mathcal{R}_1, \mathcal{R}_2, \mathcal{D}_i\}$. Here, $[\boldsymbol{\lambda}_k]_{l_{\mathcal{A}\mathcal{B}}}$ denotes the eigenvalue of the codeword difference matrix and $\boldsymbol{\nu}_k$ is the zero-mean complex Gaussian vector with unit variance. In (31), each component of the summations of the right hand side can be expressed by either one of the two following factors

$$d_1^2 = \sum_{l_{\mathcal{R}_k\mathcal{D}_i}=1}^{L_{\mathcal{R}_k\mathcal{D}_i}} |[\mathbf{h}_{\mathcal{R}_k\mathcal{D}_i}]_{l_{\mathcal{R}_k\mathcal{D}_i}}|^2 \sum_{l_{\mathcal{S}_i\mathcal{R}_k}=1}^{L_{\mathcal{S}_i\mathcal{R}_k}} [\boldsymbol{\lambda}]_{l_{\mathcal{S}_i\mathcal{R}_k}}|[\boldsymbol{\nu}]_{l_{\mathcal{S}_i\mathcal{R}_k}}|^2, \tag{32}$$

$$d_2^2 = \sum_{l_{\mathcal{S}_i\mathcal{R}_k}=1}^{L_{\mathcal{S}_i\mathcal{R}_k}} |[\mathbf{h}_{\mathcal{S}_i\mathcal{R}_k}]_{l_{\mathcal{S}_i\mathcal{R}_k}}|^2 \sum_{l_{\mathcal{R}_k\mathcal{D}_i}=1}^{L_{\mathcal{R}_k\mathcal{D}_i}} [\boldsymbol{\lambda}]_{l_{\mathcal{R}_k\mathcal{D}_i}}|[\boldsymbol{\nu}]_{l_{\mathcal{R}_k\mathcal{D}_i}}|^2. \tag{33}$$

For simplicity of mathematical formulation, let us denote $L_{\mathcal{S}_i\mathcal{R}_k} = L_1$, $L_{\mathcal{R}_k\mathcal{D}_i} = L_2$, $\mathbf{h}_{\mathcal{S}_i\mathcal{R}_k} = \mathbf{h}_1$ and $\mathbf{h}_{\mathcal{R}_k\mathcal{D}_i} = \mathbf{h}_2$. The PEP will now be analysed for scenarios (a) and (b).

A. Scenario (a): $\mathcal{S}_i \to \{\mathcal{R}_1, \mathcal{R}_2\}$: Rician fading, $\{\mathcal{R}_1, \mathcal{R}_2\} \to \mathcal{D}_i$: Rayleigh fading

Due to the different characteristics of fading channels, there are three situations based on the relationship of L_1 and L_2.

1) Case 1 ($L_1 < L_2$): Eq. (32) is taken into consideration. Let us define $Z_1 = d_1^2 = X_1 Y_1$ where $X_1 = \sum_{l_2=1}^{L_2} |[\mathbf{h}_2]_{l_2}|^2$ and $Y_1 = \sum_{l_1=1}^{L_1} [\boldsymbol{\lambda}]_{l_1} |[\boldsymbol{\nu}]_{l_1}|^2$. Applying the Chernoff bound, the PEP corresponding to d_1^2 is upper bounded by $E_{Z_1}[\exp(-\alpha^2 Z_1/4N_0)] = \Phi_{Z_1}(s)|_{s=-\alpha^2/4N_0}$. Here, α corresponds to α_k, $k = 1, 2$, if we consider $\mathcal{R}_k$, and $\Phi_{Z_1}(s)$ can be evaluated as [21, Sect. 3.1-2]

$$\Phi_{Z_1}(s) = \int_0^\infty f_{X_1}(x_1) \Phi_{Y_1}(s x_1) dx_1, \tag{34}$$

where

$$f_{X_1}(x_1) = \frac{{L_2}^{L_2}}{\Gamma(L_2)} \frac{x_1^{L_2-1}}{e^{L_2 x_1}}, \tag{35}$$

$$\Phi_{Y_1}(s) = \prod_{l_1=1}^{L_1} \frac{1+n^2}{1+n^2 - s[\boldsymbol{\lambda}]_{l_1}} e^{\frac{n^2 s[\boldsymbol{\lambda}]_{l_1}}{1+n^2-s[\boldsymbol{\lambda}]_{l_1}}}, \tag{36}$$

where n is the Nakagami-n or Rician fading parameter and $\Gamma(\cdot)$ represents the Gamma function defined by $\Gamma(k) \triangleq (k-1)!$ for any positive integer k [22, eq. 8.339.1].

Substituting (35) and (36) into (34), we have

$$\begin{aligned} \Phi_{Z_1}(s)\big|_{s=-\frac{\alpha^2}{4N_0}} &= \int_0^\infty \frac{{L_2}^{L_2}}{\Gamma(L_2)} \frac{x_1^{L_2-1}}{e^{L_2 x_1}} \prod_{l_1=1}^{L_1} \frac{1+n^2}{1+n^2+\frac{\alpha^2}{4N_0} x_1 [\boldsymbol{\lambda}]_{l_1}} e^{\frac{-n^2 \frac{\alpha^2}{4N_0} x_1 [\boldsymbol{\lambda}]_{l_1}}{1+n^2+\frac{\alpha^2}{4N_0} x_1 [\boldsymbol{\lambda}]_{l_1}}} dx_1 \\ &= \frac{{L_2}^{L_2}}{\Gamma(L_2)} \int_0^\infty \frac{x_1^{L_2-1}}{e^{L_2 x_1}} \prod_{l_1=1}^{L_1} \frac{e^{\frac{-x_1}{\frac{x_1}{1+n^2}+\frac{1}{n^2}\frac{\alpha^2}{4N_0}[\boldsymbol{\lambda}]_{l_1}}}}{\frac{\alpha^2}{4N_0}[\boldsymbol{\lambda}]_{l_1}\left(\frac{x_1}{1+n^2}+\frac{1}{\frac{\alpha^2}{4N_0}[\boldsymbol{\lambda}]_{l_1}}\right)} dx_1. \end{aligned} \tag{37}$$

Assuming high signal-to-noise ratio (SNR), i.e. $\alpha^2/4N_0 \gg 1$, and $(1+n^2)/n^2 \approx 1$, (37) can be approximated as

$$\Phi_{Z_1}(s)\big|_{s=-\frac{\alpha^2}{4N_0}} \approx \frac{L_2^{L_2}}{\Gamma(L_2)} \left(\frac{\alpha^2}{4N_0}\right)^{-L_1} \left(\frac{1+n^2}{e^{n^2}}\right)^{L_1} \prod_{l_1=1}^{L_1} \frac{1}{[\boldsymbol{\lambda}]_{l_1}} \int_0^\infty \frac{x_1^{L_2-L_1-1}}{e^{L_2 x_1}} dx_1. \tag{38}$$

When $L_1 < L_2$, evaluating the integral in (38) [22, eq. 3.351.2], we obtain

$$\Phi_{Z_1}(s)\big|_{s=-\frac{\alpha^2}{4N_0}} \approx \left[\frac{L_2(1+n^2)}{e^{n^2}}\right]^{L_1} \frac{\Gamma(L_2-L_1)}{\Gamma(L_2)} \left(\frac{\alpha^2}{4N_0}\right)^{-L_1} \prod_{l_1=1}^{L_1} \frac{1}{[\boldsymbol{\lambda}]_{l_1}}. \tag{39}$$

2) Case 2 ($L_1 > L_2$): Let us examine (33) and define $Z_2 = d_2^2 = X_2 Y_2$ where $X_2 = \sum_{l_1=1}^{L_1} |[\mathbf{h}_1]_{l_1}|^2$ and $Y_2 = \sum_{l_2=1}^{L_2} [\boldsymbol{\lambda}]_{l_2} |[\boldsymbol{\nu}]_{l_2}|^2$. Similarly, applying the Chernoff bound, the PEP corresponding to d_2^2 is upper bounded by $E_{Z_2}[\exp(-\alpha^2 Z_2/4N_0)] = \Phi_{Z_2}(s)|_{s=-\alpha^2/4N_0}$ and $\Phi_{Z_2}(s)$ is computed by

$$\Phi_{Z_2}(s) = \int_0^\infty f_{X_2}(x_2)\, \Phi_{Y_2}(s x_2)\, dx_2, \tag{40}$$

where

$$f_{X_2}(x_2) = \frac{L_1^{\frac{3-L_1}{2}}}{n^{L_1-1}} \frac{x_2^{\frac{L_1-1}{2}} I_{L_1-1}[2L_1^{\frac{3}{2}} n x_2^{\frac{1}{2}}]}{e^{L_1^2 n^2 + L_1 x_2}}, \tag{41}$$

$$\Phi_{Y_2}(s) = \prod_{l_2=1}^{L_2} \frac{1}{1 - s[\boldsymbol{\lambda}]_{l_2}}. \tag{42}$$

Here, $I_\alpha(\beta)$ denotes the modified Bessel function of the first kind, which is defined as $I_\alpha(\beta) \triangleq \left(\frac{\beta}{2}\right)^\alpha \sum_{k=0}^{\infty} \frac{\beta^{2k}}{4^k k! \Gamma(\alpha+k+1)}$, $\alpha \in \mathbb{R}$ [22, eq. 8.406.1]. Substituting (41) and (42) into (40), we have

$$\Phi_{Z_2}(s)\big|_{s=-\frac{\alpha^2}{4N_0}} = \int_0^\infty \frac{L_1^{\frac{3-L_1}{2}} x_2^{\frac{L_1-1}{2}}}{n^{L_1-1} e^{L_1^2 n^2 + L_1 x_2}} I_{L_1-1}[2(L_1)^{\frac{3}{2}} n x_2^{\frac{1}{2}}] \prod_{l_2=1}^{L_2} \frac{1}{1 + \frac{\alpha^2}{4N_0} x_2 [\boldsymbol{\lambda}]_{l_2}} dx_2. \tag{43}$$

Under the assumption of high SNR (i.e. $\alpha^2/4N_0 \gg 1$), (43) can be approximated as

$$\Phi_{Z_2}(s)\big|_{s=-\frac{\alpha^2}{4N_0}} \approx \left(\frac{\alpha^2}{4N_0}\right)^{-L_2} \frac{L_1^{\frac{3-L_1}{2}}}{n^{L_1-1} e^{L_1^2 n^2}} \prod_{l_2=1}^{L_2} \frac{1}{[\boldsymbol{\lambda}]_{l_2}} \int_0^\infty \frac{x_2^{\frac{L_1-1}{2}-L_2} I_{L_1-1}[2L_1^{\frac{3}{2}} n x_2^{\frac{1}{2}}]}{e^{L_1 x_2}} dx_2. \tag{44}$$

Evaluating the integral in (44) when $L_1 > L_2$, after some mathematical manipulations [22, eq. 3.351.2, 6.625.3], we obtain

$$\Phi_{Z_2}(s)\big|_{s=-\frac{\alpha^2}{4N_0}} \approx \frac{L_1^{L_2} \Gamma(L_1 - L_2)}{e^{L_1^2 n^2}} {}_1\tilde{F}_1(L_1 - L_2; L_1; L_1^2 n^2) \left(\frac{\alpha^2}{4N_0}\right)^{-L_2} \prod_{l_2=1}^{L_2} \frac{1}{[\boldsymbol{\lambda}]_{l_2}}, \tag{45}$$

where ${}_1\tilde{F}_1(a; b; z)$ is the regularized hypergeometric function defined as ${}_1\tilde{F}_1(a; b; z) \triangleq \frac{1}{\Gamma(a)} \sum_{k=0}^{\infty} \frac{\Gamma(a+k)}{\Gamma(b+k)} \frac{z^k}{k!}$ [22, eq. 9.14.1].

3) Case 3 ($L_1 = L_2$): Let us consider (32), for which $\Phi_{Z_1}(s)$ can be calculated as:

$$\begin{aligned} \Phi_{Z_1}(s)\big|_{s=-\frac{\alpha^2}{4N_0}} &= \frac{L_1^{L_1}}{\Gamma(L_1) e^{L_1 n^2}} \left(\frac{\alpha^2}{4N_0}\right)^{-L_1} \prod_{l_1=1}^{L_1} \frac{1}{[\boldsymbol{\lambda}]_{l_1}} \int_0^\infty \frac{x_1^{L_1-1}}{e^{L_1 x_1} \prod_{l_1=1}^{L_1} \left(\frac{x_1}{1+n^2} + \frac{1}{\frac{\alpha^2}{4N_0}[\boldsymbol{\lambda}]_{l_1}}\right)} dx_1 \\ &= \frac{L_1^{L_1} (1+n^2)^{L_1}}{\Gamma(L_1) e^{L_1 n^2}} \left(\frac{\alpha^2}{4N_0}\right)^{-L_1} \prod_{l_1=1}^{L_1} \frac{1}{[\boldsymbol{\lambda}]_{l_1}} \int_0^\infty \frac{x_1^{L_1-1} e^{-L_1(1+n^2)x_1}}{\prod_{l_1=1}^{L_1} \left(x_1 + \frac{1}{\frac{\alpha^2}{4N_0}[\boldsymbol{\lambda}]_{l_1}}\right)} dx_1. \end{aligned} \tag{46}$$

By using some mathematical expansions and integral calculations [22, eq. 3.351.2], we obtain

$$\Phi_{Z_1}(s)\big|_{s=-\frac{\alpha^2}{4N_0}} = \left[\frac{L_1(1+n^2)}{e^{n^2}}\right]^{L_1}\left(\frac{\alpha^2}{4N_0}\right)^{-L_1}\sum_{l_1=1}^{L_1}\frac{p_{l_1}}{[\boldsymbol{\lambda}]_{l_1}{}^{L_1}}e^{\frac{L_1(n^2+1)}{\frac{\alpha^2}{4N_0}[\boldsymbol{\lambda}]_{l_1}}}\Gamma\left[1-L_1, \frac{L_1(n^2+1)}{\frac{\alpha^2}{4N_0}[\boldsymbol{\lambda}]_{l_1}}\right], \quad (47)$$

where $p_{l_1} \triangleq \prod_{l=1, l\neq l_1}^{L_1}\frac{[\boldsymbol{\lambda}]_{l_1}}{[\boldsymbol{\lambda}]_{l_1}-[\boldsymbol{\lambda}]_l}$ and $\Gamma[\alpha, x]$ is the incomplete Gamma function defined by $\Gamma[\alpha, x] \triangleq \int_x^\infty t^{\alpha-1}e^{-t}dt$ [22, eq. 8.350.2].

B. Scenario (b): $\mathcal{S}_i \to \{\mathcal{R}_1, \mathcal{R}_2\}$ and $\{\mathcal{R}_1, \mathcal{R}_2\} \to \mathcal{D}_i$: Rician fading

Let n_1 and n_2 denote the Rician fading parameters of the links $\mathcal{S}_i \to \{\mathcal{R}_1, \mathcal{R}_2\}$ and $\{\mathcal{R}_1, \mathcal{R}_2\} \to \mathcal{D}_i$, respectively. Similarly, we investigate three cases based on the relationship of L_1 and L_2.

1) Case 1 ($L_1 < L_2$): We also take into consideration (32) and evaluate $\Phi_{Z_1}(s)$ where

$$f_{X_1}(x_1) = \frac{L_2^{\frac{3-L_2}{2}}}{n_2^{L_2-1}}\frac{x_1^{\frac{L_2-1}{2}}I_{L_2-1}[2L_2^{\frac{3}{2}}n_2x_1^{\frac{1}{2}}]}{e^{L_2^2n_2^2+L_2x_1}}, \quad (48)$$

$$\Phi_{Y_1}(s) = \prod_{l_1=1}^{L_1}\frac{1+n_1^2}{1+n_1^2-s[\boldsymbol{\lambda}]_{l_1}}e^{\frac{n_1^2s[\boldsymbol{\lambda}]_{l_1}}{1+n_1^2-s[\boldsymbol{\lambda}]_{l_1}}}. \quad (49)$$

Substituting (48) and (49) into (34), we have

$$\Phi_{Z_1}(s)\big|_{s=-\frac{\alpha^2}{4N_0}} = \int_0^\infty \frac{L_2^{\frac{3-L_2}{2}}}{n_2^{L_2-1}}\frac{x_1^{\frac{L_2-1}{2}}I_{L_2-1}[2L_2^{\frac{3}{2}}n_2x_1^{\frac{1}{2}}]}{e^{L_2^2n_2^2+L_2x_1}}\prod_{l_1=1}^{L_1}\frac{1+n_1^2}{1+n_1^2+\frac{\alpha^2}{4N_0}x_1[\boldsymbol{\lambda}]_{l_1}}e^{\frac{-n_1^2\frac{\alpha^2}{4N_0}x_1[\boldsymbol{\lambda}]_{l_1}}{1+n_1^2+\frac{\alpha^2}{4N_0}x_1[\boldsymbol{\lambda}]_{l_1}}}dx_1. \quad (50)$$

Under high SNR assumptions, (50) can be approximated as

$$\Phi_{Z_1}(s)\big|_{s=-\frac{\alpha^2}{4N_0}} \approx \frac{L_2^{\frac{3-L_2}{2}}}{e^{L_2^2n_2^2+L_1n_1^2}}\frac{(1+n_1^2)^{L_1}}{n_2^{L_2-1}}\left(\frac{\alpha^2}{4N_0}\right)^{-L_1}\prod_{l_1=1}^{L_1}\frac{1}{[\boldsymbol{\lambda}]_{l_1}}\int_0^\infty\frac{x_1^{\frac{L_2-1}{2}-L_1}}{e^{L_2x_1}}I_{L_2-1}\left[2L_2^{\frac{3}{2}}n_2x_1^{\frac{1}{2}}\right]dx_1. \quad (51)$$

Calculating the integral in (51) when $L_1 < L_2$ [22, eq. 3.351.2, 6.625.3], we obtain

$$\Phi_{Z_1}(s)\big|_{s=-\frac{\alpha^2}{4N_0}} \approx \frac{[L_2(1+n_1^2)]^{L_1}}{e^{L_2^2n_2^2+L_1n_1^2}}\Gamma(L_2-L_1){}_1\tilde{F}_1\left(L_2-L_1; L_2; L_2^2n_2^2\right)\left(\frac{\alpha^2}{4N_0}\right)^{-L_1}\prod_{l_1=1}^{L_1}\frac{1}{[\boldsymbol{\lambda}]_{l_1}}. \quad (52)$$

2) Case 2 ($L_1 > L_2$): By considering (33) with the same approach as Case 1, $\Phi_{Z_2}(s)\big|_{s=-\frac{\alpha^2}{4N_0}}$ can be approximated by

$$\Phi_{Z_2}(s)\big|_{s=-\frac{\alpha^2}{4N_0}} \approx \frac{[L_1(1+n_2^2)]^{L_2}}{e^{L_1^2n_1^2+L_2n_2^2}}\Gamma(L_1-L_2){}_1\tilde{F}_1\left(L_1-L_2; L_1; L_1^2n_1^2\right)\left(\frac{\alpha^2}{4N_0}\right)^{-L_2}\prod_{l_2=1}^{L_2}\frac{1}{[\boldsymbol{\lambda}]_{l_2}}. \quad (53)$$

3) Case 3 ($L_1 = L_2$): Let us rewrite (50) as

$$\begin{aligned}\Phi_{Z_1}(s)\big|_{s=-\frac{\alpha^2}{4N_0}} &= \frac{L_1^{\frac{3-L_1}{2}}}{n_2^{L_1-1}e^{L_1^2n_2^2+L_1n_1^2}}\left(\frac{\alpha^2}{4N_0}\right)^{-L_1}\prod_{l_1=1}^{L_1}\frac{1}{[\boldsymbol{\lambda}]_{l_1}}\int_0^{\infty}\frac{x_1^{\frac{L_1-1}{2}}I_{L_1-1}[2L_1^{\frac{3}{2}}n_2x_1^{\frac{1}{2}}]}{e^{L_1x_1}\prod_{l_1=1}^{L_1}\left(\frac{x_1}{1+n_1^2}+\frac{1}{\frac{\alpha^2}{4N_0}[\boldsymbol{\lambda}]_{l_1}}\right)}dx_1 \\ &= \frac{L_1^{\frac{3-L_1}{2}}}{n_2^{L_1-1}e^{L_1^2n_2^2+L_1n_1^2}}\left(\frac{\alpha^2}{4N_0}\right)^{-L_1}\prod_{l_1=1}^{L_1}\frac{1}{[\boldsymbol{\lambda}]_{l_1}}\int_0^{\infty}\frac{x_1^{\frac{L_1-1}{2}}I_{L_1-1}[2L_1^{\frac{3}{2}}n_2(1+n_1^2)^{\frac{1}{2}}x_1^{\frac{1}{2}}]}{e^{L_1(1+n_1^2)x_1}\prod_{l_1=1}^{L_1}\left(x_1+\frac{1}{\frac{\alpha^2}{4N_0}[\boldsymbol{\lambda}]_{l_1}}\right)}dx_1.\end{aligned} \tag{54}$$

With some mathematical expansions and integral calculations [22, eq. 3.351.2, 6.625.3], we obtain

$$\Phi_{Z_1}(s)\big|_{s=-\frac{\alpha^2}{4N_0}} = \frac{L_1^{3-2L_1}}{e^{L_1^2n_2^2+L_1n_1^2}}\frac{1+n_1^2}{n_2^{2L_1-2}}\left(\frac{\alpha^2}{4N_0}\right)^{-L_1}\sum_{l_1=1}^{L_1}\frac{p_{l_1}}{[\boldsymbol{\lambda}]_{l_1}}\left[\Gamma(L_1-1,-L_1^2n_2^2)-\Gamma(L_1-1)\right]. \tag{55}$$

(OB2) Achievable Diversity Gain and Effects of Rician Fading Parameters on Performance: From the PEP analysis of fading scenario (a) with Eqs. (39), (45) and (47) and fading scenario (b) with Eqs. (52), (53) and (55), we can conclude that the diversity gain of our proposed DSTFBC for both the primary and secondary transmissions in all three fading scenarios is $\min(L_{\mathcal{S}_i\mathcal{R}_1}, L_{\mathcal{R}_1\mathcal{D}_i}) + \min(L_{\mathcal{S}_i\mathcal{R}_2}, L_{\mathcal{R}_2\mathcal{D}_i})$, $i = 0, 1, 2, \ldots, N$, by observing the exponential terms of $\frac{\alpha^2}{4N_0}$. Additionally, it can be observed that the Rician fading parameters do not produce any diversity gain, however, they play a similar function to coding gain, and thus can improve the PEP, which will be confirmed through the simulation results.

V. Simulation Results

In this section, we evaluate the uncoded BER performance of the proposed DSTFBC in an CWBRN to confirm the analysis of the achievable diversity gain. The simulation is carried out based on Example 1 using SC-FDE technique, spectrum allocation algorithm in Table I, quadrature phase shift keying (QPSK) modulation with Gray mapping for random dispersive channels. Here, QPSK is selected for ease of the simulation. The use of higher modulation would cause higher demodulation complexity, however, this is beyond the scope of this paper. The fast Fourier transform (FFT) algorithm is employed for low-complexity data detection. Each transmitted data block consists of 256 symbols including the zero sequence and modulated information-carrying data. The simulation results are obtained by using Monte Carlo simulation in MATLAB for each data transmission with a loop of 10^8 times producing a BER accuracy of less than 10^{-7}. A quasi-static fading channel model with a uniform power delay profile is considered, where the channel gains are assumed to remain constant over two time slots and

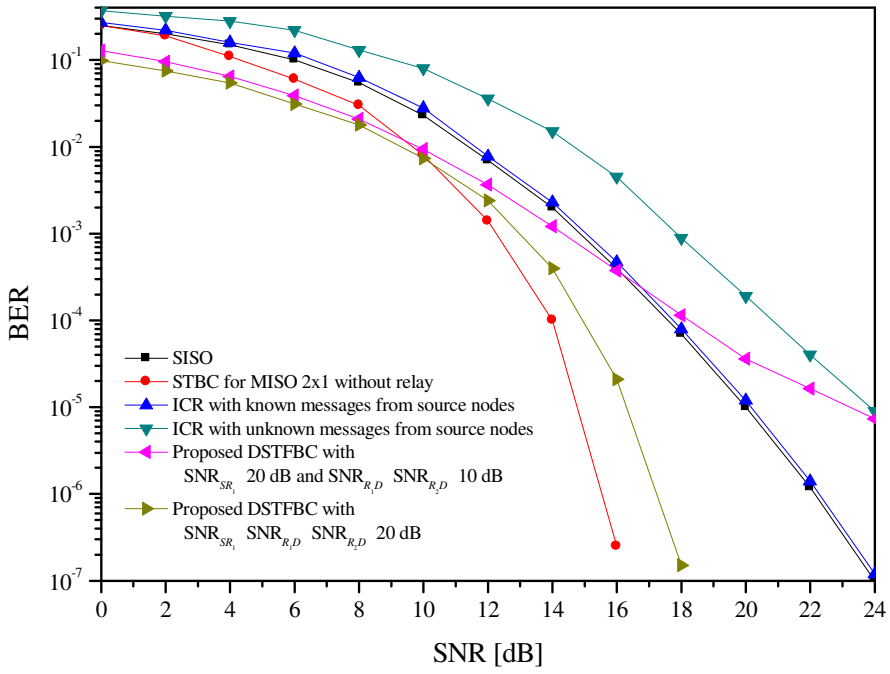

Fig. 3. Performance comparison of various transmission schemes in an CWBRN over Rayleigh frequency selective fading channels with $L_{\mathcal{S}_0\mathcal{R}_1} = 5$, $L_{\mathcal{S}_0\mathcal{R}_2} = 7$, $L_{\mathcal{R}_1\mathcal{D}_0} = 5$, $L_{\mathcal{R}_2\mathcal{D}_0} = 7$.

change independently in the consecutive two time slots. We assume that the destination nodes have perfect channel state information.

Fig. 3 shows a comparison of the BER performance of the primary transmission for various schemes: the proposed DSTFBC, single-input single-output (SISO) (e.g. [23]), STBC (e.g. [24]) and interference cancellation at the cognitive relay (ICR) (e.g. [11]). The fading of links $\mathcal{S}_0 \rightarrow \{\mathcal{R}_1, \mathcal{R}_2\}$ and $\{\mathcal{R}_1, \mathcal{R}_2\} \rightarrow \mathcal{D}_0$ are assumed to be frequency-selective Rayleigh fading where the channel memory lengths are $L_{\mathcal{S}_0\mathcal{R}_1} = 5$, $L_{\mathcal{S}_0\mathcal{R}_2} = 7$, $L_{\mathcal{R}_1\mathcal{D}_0} = 5$, $L_{\mathcal{R}_2\mathcal{D}_0} = 7$. We assume that the value of $\xi_{\mathcal{S}_0\mathcal{R}_1}/N_0$ is fixed at 20 dB, $\xi_{\mathcal{R}_1\mathcal{D}_0} = \xi_{\mathcal{R}_2\mathcal{D}_0} = \xi_{\mathcal{R}\mathcal{D}_0}$. The STBC scheme refers to the classical STBC devised for co-located antennas without cognitive relay nodes, where $\mathcal{S}_0$ is assumed to be equipped with two antennas, $\mathcal{D}_0$ with a single antenna, and each path from one antenna from $\mathcal{S}_0$ to $\mathcal{D}_0$ has 6 taps (i.e. $L_{\mathcal{S}_0\mathcal{D}_0} = 6$). For fair comparison, binary phase shift keying (BPSK) modulation is employed for both SISO and STBC schemes. The performance of STBC for a no-relay scenario is presented as a benchmark. The ICR scheme refers to the scheme where the cognitive relay helps a primary and multiple secondary users decode, precode and forward their messages to the respective primary receiver and secondary receivers using a precoding scheme at the cognitive relay for interference compensation. Here, the ICR scheme with known messages and the ICR scheme with unknown messages from the source nodes are

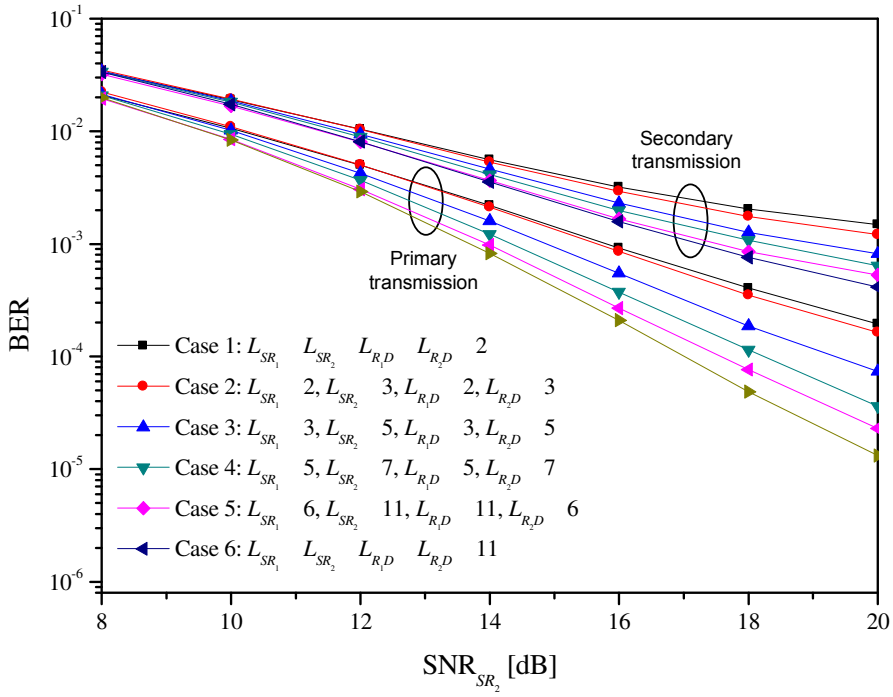

Fig. 4. BER performance of primary and secondary transmissions over Rayleigh frequency selective fading channels with various combinations of channel memory order.

both taken into consideration. In Fig. 3, SNR is referred to $\xi_{\mathcal{S}_0\mathcal{D}_0}/N_0$ for the direct transmission scenario without relay assistance, whereas it is referred to $\xi_{\mathcal{S}_0\mathcal{R}_2}/N_0$ for the relaying scenario. It can be observed that the ICR scheme with unknown messages from the sources nodes shows the worst performance. The SISO and ICR systems perform better than the DSTFBC in the high-SNR region due to the existence of an error floor when $\xi_{\mathcal{R}\mathcal{D}_0}$ is small. At high $\xi_{\mathcal{R}\mathcal{D}_0}/N_0$, the BER performance curves of the DSTFBC and conventional STBC schemes have the same slope, reflecting the same diversity order. As proved in the PEP analysis, the diversity gain of our proposed DSTFBC for the primary transmission is $\min(L_{\mathcal{S}_0\mathcal{R}_1}, L_{\mathcal{R}_1\mathcal{D}_0}) + \min(L_{\mathcal{S}_0\mathcal{R}_2}, L_{\mathcal{R}_2\mathcal{D}_0}) = 12$, which is also the maximum diversity gain of $(2 \times L_{\mathcal{S}_0\mathcal{D}_0}) = 12$ achieved with STBC.

Fig. 4 shows the BER performances of the primary and secondary transmissions as a function of $\text{SNR}_{\mathcal{S}\mathcal{R}_2}$ using the proposed DSTFBC for various combinations of channel lengths. Here, $\text{SNR}_{\mathcal{S}\mathcal{R}_2}$ represents $\xi_{\mathcal{S}_0\mathcal{R}_2}/N_0$ and $\xi_{\mathcal{S}_1\mathcal{R}_2}/N_0$ of the primary and secondary transmission, respectively. For simplicity, we study the transmission of $\mathcal{S}_1$ only. The performance of the transmission of other SUs can be similarly obtained. All fading channels are Rayleigh fading. We assume that $\xi_{\mathcal{S}_0\mathcal{R}_1}/N_0 = 20$ dB, $\xi_{\mathcal{S}_1\mathcal{R}_1}/N_0 = 15$ dB, $\xi_{\mathcal{R}_1\mathcal{D}_0} = \xi_{\mathcal{R}_2\mathcal{D}_0} = \xi_{\mathcal{R}\mathcal{D}_0} = 10$ dB and $\xi_{\mathcal{R}_1\mathcal{D}_1} = \xi_{\mathcal{R}_2\mathcal{D}_1} = \xi_{\mathcal{R}\mathcal{D}_1} = 5$ dB. For the primary and secondary transmissions, the BER

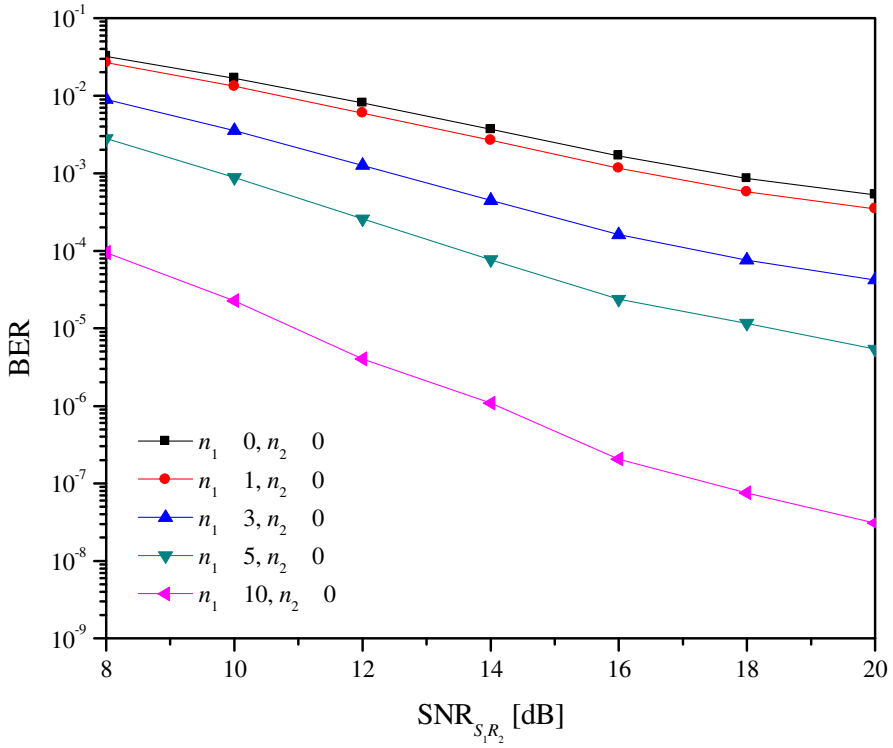

Fig. 5. BER performance of secondary transmission over mixed Rician-Rayleigh frequency selective fading channels with various Rician fading factors.

comparisons of 6 cases of different diversity orders are considered. It can be observed that the diversity gain is improved with increasing number of channel memory taps, which results in steeper BER curves. Explicitly, in Fig. 4, the curve for Case 1 has the smallest slope while the steepest curve corresponds to case 6 since Case 1 and Case 6 achieve the lowest and highest diversity gain, respectively. Also, we observe that the curves for Case 4 and Case 5 have the same slope at high SNR with the same achievable diversity order. These facts confirm our conclusion of the achievable diversity gain of the proposed DSTFBC in observation (OB2). Additionally, due to the fact that $\xi_{\mathcal{S}_0\mathcal{R}_1}/N_0 = 20$ dB and $\xi_{\mathcal{S}_1\mathcal{R}_1}/N_0 = 15$ dB, it can be seen in Fig. 4 that, in order to achieve the same target BER as with the primary transmission, a higher SNR of the link from the source to the second relay $\mathcal{R}_2$ is required.

The performance of the proposed DSTFBC for secondary transmission over wireless fading channels where the cognitive relays are located near the source nodes (i.e. scenario (a) in Section IV) is shown in Fig. 5. For this situation, the communication links $\mathcal{S}_1 \to \{\mathcal{R}_1, \mathcal{R}_2\}$ and $\{\mathcal{R}_1, \mathcal{R}_2\} \to \mathcal{D}_1$ are assumed to be LOS and NLOS, respectively, and thus the fading channels $\mathcal{S}_1 \to \{\mathcal{R}_1, \mathcal{R}_2\}$ are considered as Rician distributions and $\{\mathcal{R}_1, \mathcal{R}_2\} \to \mathcal{D}_1$ as Rayleigh distribu-

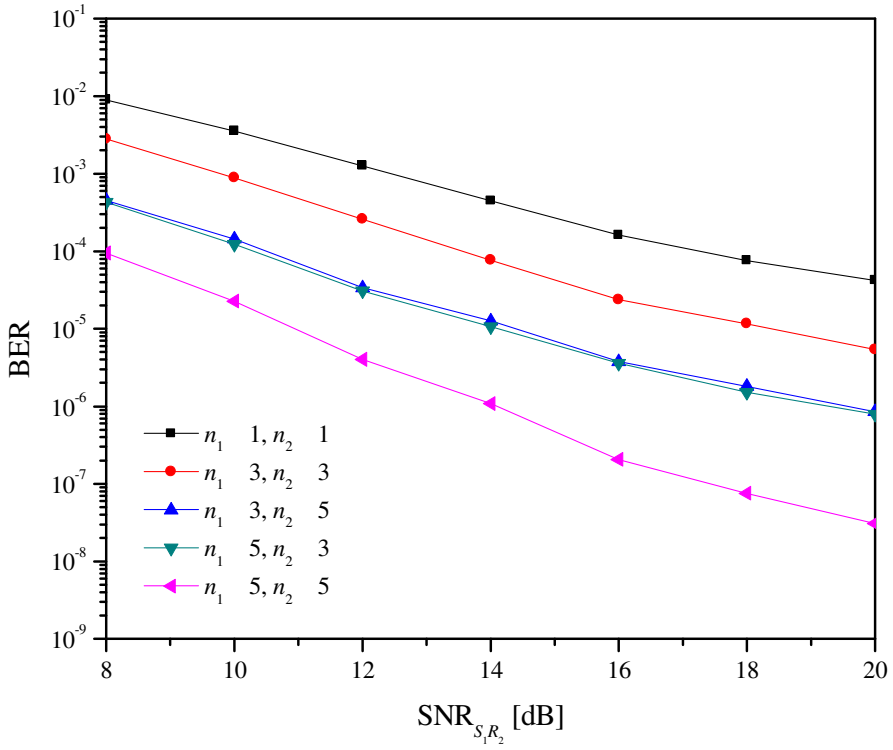

Fig. 6. BER performance of secondary transmission over Rician frequency selective fading channels with various Rician fading factors.

tions. The channel memory orders of fading channels $\mathcal{S}_1 \to \{\mathcal{R}_1, \mathcal{R}_2\}$ and $\{\mathcal{R}_1, \mathcal{R}_2\} \to \mathcal{D}_1$ are assumed to be $L_{\mathcal{S}_1\mathcal{R}_1} = 6$, $L_{\mathcal{S}_1\mathcal{R}_2} = 11$, $L_{\mathcal{R}_1\mathcal{D}_1} = 11$, $L_{\mathcal{R}_2\mathcal{D}_1} = 6$. In Fig. 5, the BER performance of the secondary transmission is plotted as a function of $\xi_{\mathcal{S}_1\mathcal{R}_2}/N_0$ with different values of Rician fading factor n_1 and n_2. Specifically, n_1 is varied as $\{0, 1, 3, 5, 10\}$ while $n_2 = 0$ since links $\{\mathcal{R}_1, \mathcal{R}_2\} \to \mathcal{D}_1$ are Rayleigh fading. The SNR values of the other links are similarly set as in Fig. 4. It can be seen that improved performance is achieved as n_1 increases. However, the slopes of the BER curves are almost the same at high SNR, which means that they achieve the same diversity gain. This can be explained as the influence of the LOS component on the BER gain through all ranges of SNR values where the Rician fading parameter only produces coding gain to the PEP as we can see in the analysis. This also confirms our conclusion about the achievable diversity gain stated in observation (OB2), which is independent of the Rician fading factor.

Let us also investigate the scenario where the cognitive relays are located near the centre of the network (i.e. scenario (b) in Section IV), where all links are assumed to be LOS, and thus characterised by Rician fading. The BER performance for secondary transmissions is plotted in

Fig. 6 as a function of $\xi_{\mathcal{S}_1\mathcal{R}_2}/N_0$ with respect to various Rician fading values n_1 and n_2, and with the same assumptions of SNR values as in Fig. 4. Specifically, five cases $\{n_1 = 1, n_2 = 1\}$, $\{n_1 = 3, n_2 = 3\}$, $\{n_1 = 3, n_2 = 5\}$, $\{n_1 = 5, n_2 = 3\}$ and $\{n_1 = 5, n_2 = 5\}$ are considered as examples. The channel memory orders of fading channels $\mathcal{S}_1 \to \{\mathcal{R}_1, \mathcal{R}_2\}$ and $\{\mathcal{R}_1, \mathcal{R}_2\} \to \mathcal{D}_1$ are assumed as in Fig. 5. Similarly, it can be observed that the BER curves have the same slopes at high SNR and a reduced BER is always achieved when either n_1 or n_2 increases. Specifically, the BER curves are only shifted down if we increase either n_1 or n_2. This means that they achieve the same diversity gain, however, the increased Rician fading factor provides further coding gain to the BER performance. This again confirms our statement in observation (OB2) regarding the achievable diversity gain, which depends only on the channel memory lengths.

VI. Conclusions

In this paper, we proposed a new DSTFBC scheme for two-hop cognitive wireless broadband relay systems, which achieves a spatial diversity order of $\min(L_{\mathcal{S}_i\mathcal{R}_1},\ L_{\mathcal{R}_1\mathcal{D}_i}) + \min(L_{\mathcal{S}_i\mathcal{R}_2},\ L_{\mathcal{R}_2\mathcal{D}_i})$, $i = 0, 1, 2, \ldots, N$, for both primary and secondary transmissions. In addition, this DSTFBC design allows the data detection to be decoupled in the frequency domain for a low-complexity receiver. Furthermore, the PEP performance has been analysed for various scenarios of cognitive relay location represented by mixed Rayleigh and Rician frequency-selective fading channels. The analysis and simulation results have validated the theoretically derived diversity order and have shown that the LOS component in Rician fading effectively improves the error rate performance at the destination nodes. For future work, we will theoretically evaluate the error floor of our proposed DSTFBC in the CWBRN context.

References

[1] Mitola, I.J., Maguire, J.G.Q.: 'Cognitive radio: Making software radios more personal', *IEEE Pers. Commun.*, 1999, 6, (4), pp. 13-18.

[2] Wang, J., Ghosh, M., Challapali, K.: 'Emerging cognitive radio applications: A survey', *IEEE Commun. Mag.*, 2011, 49, (3), pp. 74–81.

[3] Telatar, E.: 'Capacity of multi-antenna Gaussian channels', *Eur. Trans. Telecommun.*, 1999, 10, (6), pp. 585–596.

[4] Laneman, J., Wornell, G.: 'Distributed space-time-coded protocols for exploiting cooperative diversity in wireless networks', *IEEE Trans. Inf. Theory*, 2003, 49, (10), pp. 2415–2425.

[5] Tarokh, V., Jafarkhani, H., Calderbank, A.: 'Space-time block codes from orthogonal designs', *IEEE Trans. Inf. Theory*, 1999, 45, (5), pp. 1456–1467.

[6] Jing, Y., Hassibi, B.: 'Distributed space-time coding in wireless relay networks', *IEEE Trans. Wireless Commun.*, 2006, 5, (12), pp. 3524–3536.

[7] Yang, W., Cai, Y., Zheng, B.: 'Distributed space-time-frequency coding for broadband wireless relay networks', *IEEE Trans. Veh. Technol.*, 2012, 61, (1), pp. 15–21.

[8] Wu, J., Hu, H., Uysal, M.: 'High-rate distributed space-time-frequency coding for wireless cooperative networks', *IEEE Trans. Wireless Commun.*, 2011, 10, (2), pp. 614–625.

[9] Letaief, K.B., Zhang, W.: 'Cooperative communications for cognitive radio networks', *Proc. of the IEEE*, 2009, 97, (5), pp. 878–893.

[10] Zou, Y., Zhu, J., Zheng, B., Yao, Y.-D.: 'An adaptive cooperation diversity scheme with best-relay selection in cognitive radio networks', *IEEE Trans. Signal Process.*, 2010, 58, (10), pp. 5438–5445.

[11] Sarkar, M., Ratnarajah, T., Sellathurai, M.: 'Outage performance of MIMO multiple access interference channel with cognitive relay'. IEEE ICC 2010, Cape Town, South Africa, 2010, pp. 1–5.

[12] Falconer, D., Ariyavisitakul, S.L., Benyamin-Seeyar, A., Eidson, B.: 'Frequency domain equalization for single-carrier broadband wireless systems', IEEE Commun. Mag., 2002, 40, (4), pp. 58–66.

[13] Laneman, J., Tse, D., Wornell, G.: 'Cooperative diversity in wireless networks: Efficient protocols and outage behavior', *IEEE Trans. Inf. Theory*, 2004, 50, (12), pp. 3062–3080.

[14] Yucek, T., Arslan, H.: 'A survey of spectrum sensing algorithms for cognitive radio applications', *IEEE Commun. Surveys and Tutorials*, 2009, 11, (1), pp. 116–130.

[15] Zhang, W., Letaief, K.: 'Cooperative spectrum sensing with transmit and relay diversity in cognitive radio networks', *IEEE Trans. Wireless Commun.*, 2008, 7, (12), pp. 4761–4766.

[16] Vien, Q.-T., Stewart, B.G., Tianfield, H., Nguyen, H.X.: 'Efficient cooperative spectrum sensing for three-hop cognitive wireless relay networks', *IET Commun.*, 2013, 7, (2), pp. 119–127.

[17] Digham, F.F., Alouini, M.-S., Simon, M.K.: 'On the energy detection of unknown signals over fading channels', *IEEE Trans. Commun.*, 2007, 55, (1), pp. 21–24.

[18] Gan, X., Chen, B.: 'A novel sensing scheme for dynamic multichannel access', *IEEE Trans. Veh. Technol.*, 2012, 61, (1), pp. 208–221.

[19] Simon, M. K., Alouini, M.-S.: 'Digital Communication over Fading Channels' (John Wiley & Sons, 2005, 2nd edn.).

[20] Proakis, J.G.: 'Digital Communications' (McGraw Hill, 2001, 4th edn.).

[21] Stuart, A., Ord, J.K.: 'Kendall's advanced theory of statistics' (C. Griffin, London, U.K., 1987, 4th edn.)

[22] Gradshteyn, I.S., Ryzhik, I.M.: 'Table of Integrals, Series, and Products' (Academic Press, 2007, 7th edn.)

[23] Benvenuto, N., Tomasin, S.: 'Block iterative DFE for single carrier modulation', *IEE Electro. Lett.*, 2002, 39, (19), pp. 1144–1145.

[24] Zhu, Y., Letaief, K.: 'Single-carrier frequency-domain equalization with decision-feedback processing for time-reversal space-time block-coded systems', *IEEE Trans. Commun.*, 2005, 53, (7), pp. 1127–1131.